Technische Universität München
Lehrstuhl für Elektrische Energiespeichertechnik
Prof. Dr.-Ing. Andreas Jossen

Performance analysis of packaging geometries of $LiFePO_4$ | Graphite (LFPC) cells

Master thesis

of

Ayush Sengupta

Supervisor:
Dipl.-Ing. Ms. Yao Wu

DD. MMMM YYYY

Abstract

Please write a brief abstract before your index.

Following aspects are supposed to be mentioned:

- Briefly describe your motivation/present the problem
- Aims and tasks of the thesis
- Essential results
- If applicable, limitation of the thesis

This paragraph is usually the first page one will see, please be very diligent! The summary shall not be mistaken for the instruction and it should not describe the structure of the thesis.

Abstract

$LiFePO_4$ | Graphite cells are gaining popularity among lithium battery technologies because of added safety and potential to be low cost. But it still suffers from disadvantages like reduced energy and power density. While lot of research is going on to improve these cells, the research on the impact of packaging geometries on the cell properties is still minimal. While cylindrical and prismatic cells are the most popular, pouch cells are relatively less matured as a technology despite the advantages of higher energy density and flexibility. Commercially, cells of the three geometries have different chemical composition and different rated capacities which makes an accurate comparison much difficult. This thesis aims to analyze the performance and effect of different packaging geometries of cells manufactured specifically with a common chemistry and to deliver the same rated capacities.

The thesis was restricted to cyclic aging tests. First the performance of unaged cells (100% SOH) conditioned at 0.3C, 5°C were analyzed with respect to DC pulsed tests for segregating the internal resistances and polarizations, and temperature developed over the cycles. It was observed that pouch cells showed the least internal resistances while prismatic cells showed the highest. Pouch cells showed a very steep rise in internal resistances at the end of the discharge cycle. The temperature rise was relatively low due to a low maximum C-rate of 2C for cycling (maximum 10.40K increase for prismatic cells). As expected from the trend of ohmic resistances, prismatic cells reached highest temperatures with pouch cells showing the lowest high temperatures. The study of aging mechanisms showed evidence of early stage Lithium plating for cylindrical and prismatic cells at low temperatures of cycling, and possibility of loss of active material (LAM) at later stages due to electrode deterioration. Pouch cells showed the best capacity retention and evidence to prove the most stable and uniform SEI layer formation. The optimum temperature of cycling was found to be highest for cylindrical cells and least for pouch cells. DC pulsed tests of aged cells showed very large variations in resistance values for pouch cells with respect to a new cell. A rapid increase in internal resistance in the case of pouch cell was found to set in at a very latter stage as compared to the other two geometries. In the end, the thesis also discusses strategies for a more thorough comparison of the geometries. The main purpose of the work is to pave way for further research in this particular area and extend it to practical applications.

Index

Abrieviation register

DOD ..... *Depth of Discharge*
DVA ..... *Differential Voltage Analysis*
ECU ..... *Extended Check-Up*
EFC ..... *Equivalent Full Cycles*
ESS ..... *Energy Storage Systems*
EV ..... *ELectric Vehicles*
GIC ..... *Graphite Intercalated Compound*
HEV ..... *Hybrid Electric Vehicles*
IRR ..... *Internal Resistance Ratio*
LAM ..... *Loss of Active Material*
LFPC ..... *Lithium Ferrous Phosphate- Carbon*
LLI ..... *Loss of Lithium Inventory*
OCV ..... *Open Circuit Voltage*
ORI ..... *Ohmic Resistance Increase*
SCU ..... *Short Check-Up*
SEI ..... *Solid Electrolyte Interface*
SOC ..... *State of Charge*
XCTS ..... *Extended Cell Test System*

1 Introduction

With the world moving towards consumer electronics, automation and smart technologies, battery energy storage to run these systems has become even more important. Among all, Lithium-ion battery technologies have found applications from small consumer electronics to large stationary storage systems. Use of lithium-ion batteries is on the rise especially in the case of electric vehicles or EVs (including hybrid electric vehicles HEV) with humans consciously moving towards a greener future. Due to its chemical properties, lithium-ion can be used in a variety of electrode configuration which makes it suitable for different applications. The lithium-ion batteries used with EVs are very expensive. This necessitates the need for further research on reducing costs and achieving optimal functionality. Another important aspect to be taken care of are the safety issues with many of the early lithium-ion technologies prone to overheating which not only damages the battery itself but also can be hazardous. The collaborative research project, SPICY aims at development of new generation of lithium-ion batteries with respect to performance, safety, costs, recyclability and lifetime. It particularly involves performance improvement of $LiFePO_4$ based Lithium Ferrous Phosphate-Carbon cells (LFPC). All the test data for the thesis have been obtained from SPICY partners.

$LiFePO_4$ is well known as a safer and more durable than other cathode materials like $LiCoO_2$. Unfortunately, its energy density is low due to the electrochemical potential of Fe. The LFPC cells are available in different packaging geometries: cylindrical, prismatic and pouch. These geometries offer different capabilities with some well-known properties like difference in weight, energy density and packaging efficiencies. Different EV manufacturers themselves use different packaging geometries for their vehicles. Nissan Leaf and BMW i3 are known to use the prismatic packaged cells. [1] The electric vehicle pioneer, Tesla Motors, uses cells with a cylindrical packaging (traditionally 18650 dimensions and more recently 21700 dimensions). [2] Production vehicles such as Daimler Smart, Renault Zoe and Nissan Leaf as well use cells with pouch type packaging geometry. [2]

While each design has clear advantages and disadvantages, there is no winner on overall performance for mass-market EVs. [3] Cylindrical cells are still the most matured technology compared to the others. While use of prismatic cells is also on the rise for different battery

technologies, pouch cells are only used for the case of lithium-ion cells and was introduced for its reduced weight. Research has been done for many different commercial cells with respect to their performance, safety and reliability concerns for e.g. the temperature developed or the capacity deterioration mechanism. These also include research on different commercial cells of different geometries. But this does not provide a fair comparison of the performance of the cells in different geometries as the commercial cells researched and compared are either of different chemical composition or have different designed capacities. Dedicated research based on performance and aging of cells is lacking for the different packaging geometries which have the same chemical composition and deliver the same capacities. Therefore, the core purpose of the thesis is to analyze cells which are based on the $LiFePO_4$|Graphite electrodes and a design capacity of 16 Ah but differ only in their packaging geometries and the results of which should logically compare the packaging geometries. As a long-term scope, the results can help further research which may eventually determine the suitability of geometries for different application.

During the thesis, the data was obtained from various tests performed by different partner organizations of the SPICY project, as mentioned earlier. State-of-the-art methods were used for the cell manufacture itself and care was taken to maintain uniformity with respect to chemistry and capacity sizing of the various geometries for a fair comparison. The data obtained was then sorted, analyzed and visualized using software like EC-Lab and MATLAB. Several assumptions were made across the cell analysis for ease of comparison and data visualization. Further, the experimental results were attempted to be validated or inference were made based on previous research by peers.

The thesis is arranged into different chapters. First, the basics of lithium-ion technology is discussed especially with respect to $LiFePO_4$|Graphite based cells and a discussion on the different geometries of packaging and the existing knowledge about their comparison. The next chapter discusses the state-of-the-art in the research on performance analysis of the geometries of the cell. It also includes a discussion of the literature on the performance and aging mechanism evaluators of Lithium-ion cells, especially those relevant to the thesis work. In the subsequent chapter, the different cells used during the experiments are described followed by detailing the specific experiments setup. This is followed by discussion of the experiment results and inference based on the literature reviewed before. The core part of the thesis ends with conclusions drawn from the results, a discussion on limitations within the work and the scope for future research and improvements.

2 Lithium-ion batteries and packaging geometries

This chapter briefly introduces the lithium-ion battery technology in general, followed by a discussion of the $LiFePO_4$|Graphite based cells and an introduction to the packaging geometries. This chapter serves as the knowledge foundation for the rest of the work.

2.1 Lithium-ion technology

Lithium-ion batteries play a significant role in present day energy storage systems, primarily due to their high energy density and high specific energy. Invented by the American physicist Professor John Goodenough in 1980 as a new type of battery in which the lithium (Li) could transport through the battery from one electrode to the other as a Li^+ ion, it was first commercially introduced as a product by Sony Corporation. [4]; [5] The simple basis of these batteries is that a compound of lithium with a transition metal - such as nickel, manganese, cobalt, iron - and oxygen forms the cathode, whereas, graphite is the anode. [4]

The chemical properties of lithium make it advantageous over other technologies. Due to its lowest reduction potential of all elements, lithium-ion cells have the highest available cell potential. Being one of the lightest element and having one of the smallest radii, lithium-based batteries have high gravimetric and volumetric capacity and power density. [6] Therefore, despite disadvantages like high costs and possible high temperature development, the above advantages make it very desirable for many commercial and research-related activities. This prompts for further studies and experiments to improve safety and reducing the costs of lithium-ion batteries.

Lithium-ion batteries are made of lithium and graphite-based electrodes, making them lighter than other types of rechargeable batteries. Lithium is highly reactive and has potential to store high energies. Lithium-ion batteries hold their charge for longer periods of time, that is they have low self-discharge. No memory effect, which means that Lithium-ion batteries do not have to be completely discharged before recharging to retain full charge capacity, which is the case in some battery chemistries like NiCd. Lithium-ion batteries have long cycle lives and can retain large number of charge-discharge cycles without significant losses in capacity. [7]

However, lithium-ion cells have a few disadvantages as well. The service life or shelf life of a lithium-ion battery decreases with aging even if it is not used. This means that from the time of manufacturing, regardless of the number of times it was cycled, the capacity of a lithium-ion battery will decline gradually. This is due to an increase in internal resistance, which makes the problem more pronounced in high-current applications. They are more sensitive to high temperatures than most other chemistries. Hot storage and operating conditions causes lithium-ion battery packs to degrade much faster than they normally would. Lithium-ion batteries can be severely damaged by deep discharge, i.e., by discharging them below the minimum voltage threshold recommended by the manufacturer. Consequently, Lithium-ion battery packs come with an on-board circuit to manage the battery. This makes them even more expensive than they already are. In general, lithium-ion chemistry is not as safe as NiCd or NiMH. This is because the anode produces heat during use, while the cathode produces oxygen (though not for all lithium-ion chemistries). Lithium being highly reactive, the lithium ions can combine with this oxygen, leading to the possibility of the battery catching on fire. [7] The safety problem in lithium-ion batteries has been attributed to thermal runaway. It is initiated by a powerful exothermic reaction of recombination of atomic hydrogen accumulated in anode graphite during the cell cycling. [8] Table 2.1 shows a comparison of Lithium-ion batteries with other technologies.

Table 2.1. Comparison of different battery technologies [9]

Cathode	**Lithium-ion**	**Pb-acid**	**Ni-Cd**	**Ni-MH**
Cycle life	500-1000	200-500	500	500
Working potential (V)	3.6	1.0	1.2	1.2
Specific energy (Wh/kg)	100	30	60	70
Specific energy (Wh/L)	240	100	155	190

Currently, lithium-ion technologies are used in a variety of applications, especially in portable electronics, EVs and power tools. The high energy efficiency of lithium-ion batteries makes them useful electric grids, where they contribute to the quality of energy harvested from wind, solar, geo-thermal and other renewable sources. It helps in more widespread use of renewable energy sources and building an energy-sustainable economy. [6]

Because of lithium's ability to form compounds with a variety of transition metals and oxygen, different types of Li battery technologies are available. Table 2.2 shows some typical properties and applications of the most commonly used types of lithium-ion batteries:

Table 2.2. Typical properties and applications of different types of lithium-ion cells [10]

	Li-Cobalt (LCO)	**Li-Manganese (LMO)**	**Li-Nickel Manganese Cobalt (LNMC)**	**Li-Iron Phosphate (LFP)**
Specific energy (Wh/kg)	150-200	100-150	150-220	90-120
Nominal voltage (V)	3.6	3.7	3.7	3.3
Cycle life	500-1000	300-700	1000-2000	1000-2000
Application	Mobile phones, tablets, laptops, cameras	Power tools, medical devices, electric powertrains	E-bikes, medical devices, EVs, industrial	Portable and stationary needing high load currents and endurance

The advantages of lithium-ion cells far outweigh the disadvantages in terms of commercial usage which necessitates the need for research to understand and alleviate the shortcomings of the technology. Such research work led to the development of $LiFePO_4$|C (LFPC) cells which is known to be low cost and offers safety, stability and well-defined performance. LFPC or $LiFePO_4$ | Graphite cells form the basis of studies in this thesis. The next subsection introduces and discusses a typical $LiFePO_4$ | Graphite cell, its geometry and chemistry in general.

2.2 $LiFePO_4$ | Graphite cells

John B. Goodenough research group at the University of Texas first published a literature in 1996 about the use of $LiFePO_4$ as an electrode for lithium-ion cells. [11] With a higher specific capacity compared to other technologies and a well-defined performance, $LiFePO_4$ | Graphite cells have found application in EVs, stationary storage systems, power backup systems etc. [12] Despite disadvantages like low electrical conductivity and slow lithium-ion diffusion, $LiFePO_4$ | Graphite is one of the safest lithium-ion technologies. It consists of $LiFePO_4$ as the cathode along with a graphitic carbon electrode in a metallic current collector grid as the anode. $LiFePO_4$ based cathodes, while having less energy density, have larger power density and better longevity as compared to other cathode materials like $LiCoO_2$. [13] To further discuss the chemistry of $LiFePO_4$ | Graphite cells, Figure 2.1 introduces a schematic of the ion-transport in the cell.

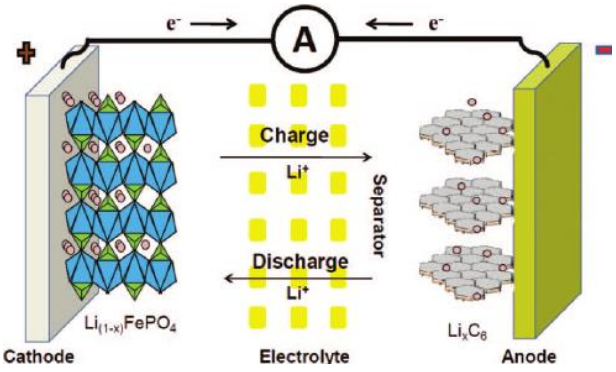

Figure 2.1. Schematic of ion-transport in a $LiFePO_4$/C cell [14]

Each cell consists of an anode of graphite on copper terminals and a cathode of $LiFePO_4$ on aluminum terminal. They are separated by an electrolyte containing dissociated lithium salts (for example, $LiPF_6$ in ethylene carbonate/dimethyl carbonate), which enables transfer of lithium ions between the two electrodes. [13] [14] The separator isolates the two electrodes and is a membrane that allows transfer of ions from cathode to anode on charge (reverse on discharge).

Equation (2.1) below represents the general chemical reaction in a $LiFePO_4$ based cell. While the forward process shows the extraction of lithium-ion to charge the cathode, the reverse process shows the discharge process. [9]

$$LiFePO_4 - x\,Li^+ - x\,e^- \leftrightharpoons x\,FePO_4 + (1-x)\,LiFePO_4 \tag{2.1}$$

The chemical reaction has been broken down to part reactions in Figure 2.2:

$LiFePO_4 \leftrightharpoons FePO_4 + Li^+ + e^-$		$Li^+ + e^- + 6C \leftrightharpoons LiC_6$
Cathode ($LiFePO_4$ on Al terminal)	**Electrolyte** $LiPF_6$ in ethylene carbonate (EC)/ dimethyl carbonate (DMC)	**Anode** (Graphite on Cu terminal)
Left to right → Charging		Right to left ← Discharging

Figure 2.2. Part reactions involved in the chemistry of an LFPC cell [13]

Figure 2.2 helps understand the reactions taking place at each of the electrodes during charging and discharging, which is essential to explain the ion-electron movement across the cell and related electrochemical processes and resistances involved.

2.3 Packaging geometries of Lithium-ion cells

The main aim of this thesis is to compare the different packaging geometries of lithium-ion cells. Most large secondary batteries are available in either prismatic or cylindrical configurations, while pouch type configuration is only present for lithium-ion cells. This sub-section, a briefly introduces and compares the geometries. Figure 2.3 shows components of the different geometries of lithium-ion cells.

Cylindrical geometry is the most common packaging technique for both primary and secondary cells. It has the main advantages of ease of manufacture and good mechanical stability. The tubular cylinder can withstand high internal pressures without deforming. Though the cylindrical cell does not fully utilize the space by creating air cavities on side-by-side placement. Despite that, among all the commercial cells available today in the market, cylindrical cells are the most matured technology and provide the highest energy density. The higher energy density of the cylindrical cell compensates for its less ideal stacking abilities and the empty space can be used for cooling to improve thermal management. This cell design allows for added safety features that are not possible with other formats. It cycles well, offers a long calendar life and is low cost, but it has less than ideal packaging density. It is available in several different geometrical sizes, with the 18650 type being the most popular. The nomenclature 18650 refers to an 18mm diameter, a 65mm height, while the last 0 refers to a cylindrical cell conforming to the IEC standards. The other Lithium-ion formats commonly available commercially are 20700, 21700 and 22700. [15]

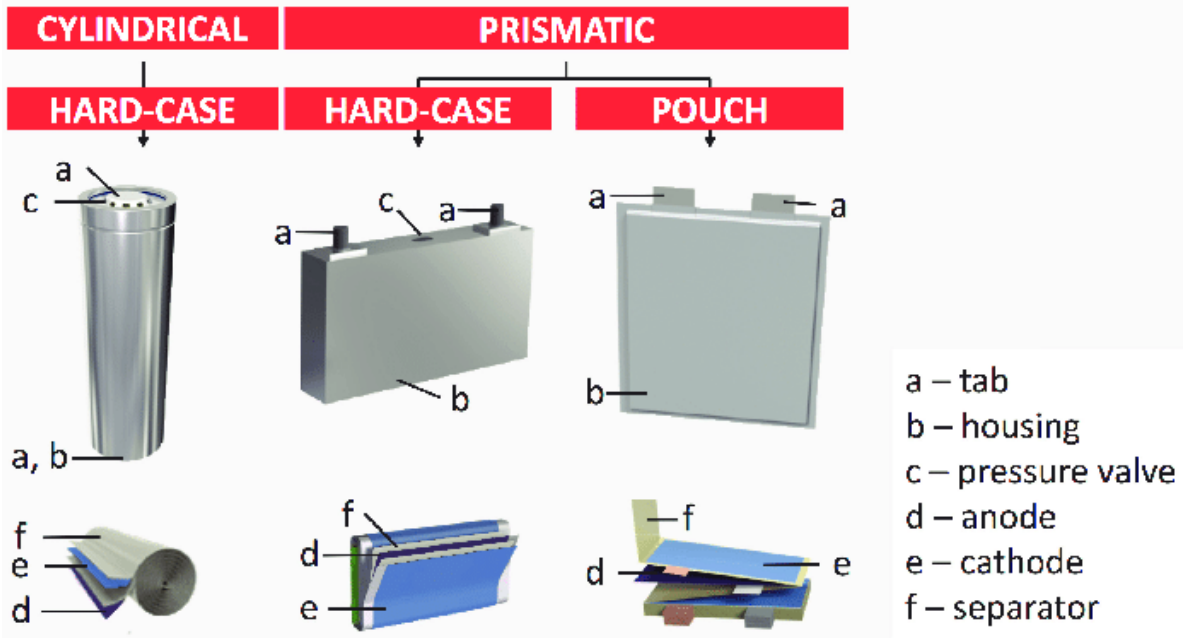

Figure 2.3. Diagram showing different geometries of Lithium-ion batteries [16]

Prismatic cells are encased in aluminum or steel for stability. Jelly-rolled or stacked, the cell is space-efficient but can be costlier to manufacture than the cylindrical cell. The prismatic cell improves space utilization and allows flexible design but it can be more expensive to manufacture, less efficient in thermal management and have a shorter cycle life than the cylindrical design. [15]

The pouch cell offers a simple, flexible and lightweight solution to battery design. Some stack pressure is recommended but allowance for swelling must be made. The pouch cells can deliver high currents, but it performs best under light loading conditions and with moderate charging. It is cost-effective but exposure to humidity and high temperature can shorten life. Adding a light stack pressure prolongs longevity by preventing delamination. Swelling of 8–10 percent over 500 cycles must be considered with some cell designs. It has been estimated that in the future pouch cells will become cheapest to manufacture. [15]

It has already been discussed that cylindrical cells are used in Tesla Motors electric vehicles, while prismatic cells are common in BMW i3 and pouch type geometry are used Daimler Smart and Renault Zoe. The following three figures show the arrangements of these geometries into battery packs in different EV-HEV cars.

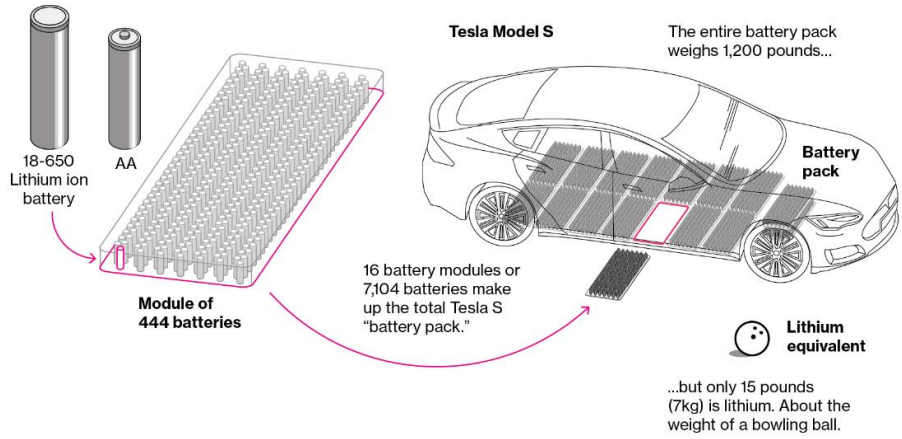

(a)

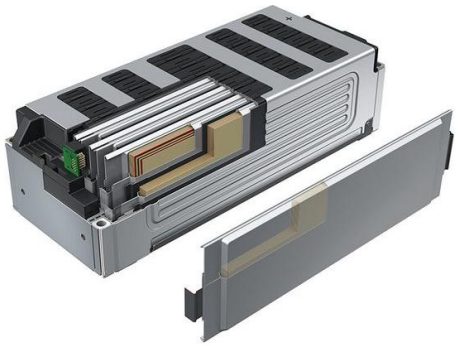

(b)

(c)

Figure 2.4. Battery pack arrangement for (a) Cylindrical [17], (b) Pouch [18], (c) Prismatic cells [18]

Figure 2.4 shows a diagram of 18650 cylindrical cell battery pack for the Tesla S model. Figure 2.4b and Figure 2.4c show the pouch and prismatic cell battery packs which are being developed by AUDI for their future electric cars. While the cylindrical cells leave behind some space from one cell to another due to their cylindrical shape, prismatic and pouch geometries show a more compact packaging, with the thin pouches providing scope for more flexibility.

While use of these geometries in different EVs has already been discussed, they find different applications in other fields as well. Cylindrical cells mostly find use in portable

applications and are used in power tools, medical instruments, laptops and e-bikes. Prismatic cells are popular in Mobiles phones, tablets and low-profile laptops electric powertrains, solar/wind storage UPS. Pouch cells are also used portable applications like drones and hobby gadgets and in energy storage systems (ESS). Standardized pouch cells are not available and it gives the manufacturers the flexibility to design to their specific needs. [19] Each cell geometry has its own pros and cons in each application but currently, the scope itself is limited by the maturity of technologies with cylindrical cells being the most advanced and researched. Table 2.3 summarizes the advantages and disadvantages of each type of cell geometry.

Table 2.3. Comparison of cell packaging geometries [19]

Cylindrical	**Prismatic**	**Pouch**
+ Ease of manufacture + Good mechanical stability + Withstand high internal pressure without deforming + Lower cost (watt per hour) + Long calendar life and cycling ability + Higher energy density	+ Thin profile (effective use of space) + Allows flexible design + Encased in metal or steel for stability	+ No need for metallic casing + Most efficient use of space + Light weight
- Notable space between cells (less space efficiency) - Heavy - Low packaging density due to space cavities	- Expensive to manufacture - Less efficient in thermal management - Shorter cycle life - Deforms at high pressure - Higher cost (watt/hour)	- Provision for swelling must be made - Cons like prismatic structure

3 State-of-the-art

Lithium-ion cells are taking over the storage market from low power to high power applications. As discussed already, due to the chemical properties of lithium, these cells can be produced with many different configurations of cathodes and anodes and in various sizes. There is further proof of benefits of using $LiFePO_4$ based cathodes. Many studies have been done to compare the different chemistries and different sizes of lithium-ion cells.

On the other hand, studies on the packaging geometries of the Lithium-ion cells are limited. Pouch based packaging geometries, for e.g., are finding lot of applications in EVs and HEVs and are even replacing cylindrical cells in many cases because of low weights and the improved energy density. Very few studies include a thorough comparison based on their performance analysis with respect to parameters like capacity evolution, internal resistance developed, differences in chemical changes during cycling. This chapter discusses the state-of-the-art in research for the comparison study between the cell packaging geometries. The literature reviewed in this study is not just limited to LFPC and lithium-ion cells but tries to incorporate relatable results from the work on other electrochemical cells as well.

3.1 Literature review on packaging geometry comparison

A physical and geometrical comparison of the three packaging types can be found in the work done by Lee et al. They have compared the physical constraints of jelly roll wound types (cylindrical and prismatic) with flat stacked designs (pouch) for lithium-polymer cells. In the case of jelly roll configurations, the metal enclosure of slimmer batteries (for e.g. prismatic cells) do not exert enough pressure onto the electrodes and this results in poor thickness control. The study also enumerates some of the advantages of a flat design: maintaining uniform battery thickness, higher energy densities due lower dead volume and lower cell impedance due to the plurality of electrical contacts through electrode tabs. Further, free stack structures without any folding options (referring to pouch type cells) allow the separator materials to contract when exposed to shutdown temperatures. This helps in triggering safety events more easily around the electrode edges. The work illustrates the need for studying of cell designs for safer lithium-ion battery technology. [20]

The work by Maiser gives a brief overview of battery packaging concepts, their specific advantages and drawbacks, as well as the influence of packaging on the performance and cost. It concludes that while the front-end production has the highest impact on the cost of the battery, back-end design and processing (packaging) adds important safety and intelligent control features without which lithium-ion batteries would not be manageable. It also

reviews a brief history, characteristics and applications of the three packaging geometries relevant to this work: cylindrical, prismatic and pouch. [21]

Mulder et al. have done a comprehensive study on the comparison of commercial lithium-ion battery technologies with different chemistries and packaging geometries. The work evaluates the behavior of these cells for automotive applications like plug-in hybrid vehicles and battery electric vehicles, where tests for high power and high energy applications are included. Within the scope of this study, commercial cells of different geometries were also studied, and a comparison was made. It was concluded that pouch cells behave better than average with respect to the power efficiency, whereas due to design factors, the prismatic shape has a clear negative effect on the efficiency. Prismatic cells also seem to have a clear negative effect on efficiency, as it becomes the hottest, while cylindrical cells warm up less. Further, pouch cells show the highest power densities. While this work is comprehensive and includes many parameters for comparison, it does not necessarily include whether the cells from the three packaging geometries have the same internal chemical composition and design capacities. [22] Therefore this work does not serve as a dedicated comparison of the three geometries.

Further literature studied for the thesis involved studies on capacity evolution, aging parameters, internal resistances, temperature developed and pulse polarization tests of lithium-ion cells. The following part discuss in detail the various aspects related to capacity deterioration and overpotentials along with the associated resistances.

3.2 Capacity deterioration

The cyclic aging and capacity deterioration of lithium-ion cells depends on a variety of factors as listed by Zhao: loss of lithium-ion-inventory, loss of active material, ohmic resistance increase, lithium plating among others. [23] These mechanisms are discussed further in detail by González. [24] Barré et al. have reviewed the aging mechanism and aging battery estimation methods in lithium-ion batteries. [25] Sarasketa-Zabala et al. provide a detailed analysis of the influence of depth of discharge (DOD), C-rate and Ah-throughput on cell aging of LFPC cells. [26] Pinson discusses the theory of solid electrolyte interface (SEI) in rechargeable batteries: capacity fade, accelerated aging and lifetime prediction. [27]

Many literatures study the aging characteristics of lithium-ions cells and discuss the involved mechanisms, although the mechanisms may differ from one chemistry and cell geometry to other. The work done by Sikha et al. discusses the capacity fade of cylindrical 18650 Lithium-ion cells at different charge-discharge protocol. For the constant current – constant voltage

(CC+CV) and constant voltage (CV) protocol, that has been used in this thesis work, the short time during which the current is very high while charging using CV protocol is responsible for increased capacity fade. [28]

Most of the known work in the case of understanding the aging behavior involve study of commercial cylindrical cells. Han et al. investigated different commercial lithium-ion cells and concluded that the aging mechanism differ with different chemistries of the cells. Two LFPC cells were investigated in this study. For one cell, it was observed that the battery aging mainly arises from the loss of lithium inventory and loss of the anode active material. While in another case, despite lithium inventory loss, no significant anode or cathode loss was observed. [29] Sun et al. studied the degradation mechanism with respect to the cycle lifetime of commercial $LiFePO_4$ | Graphite cells at different ambient temperatures and observed that the mechanism changes for different temperatures. While at room temperatures, the capacity fade is due to active lithium loss by generation and reformation of solid electrolyte interface (SEI) film, at temperatures above 35°C, the electrolyte decomposes which results in accelerated consumption of active lithium. Elevated temperatures have an adverse influence on the performance of $LiFePO_4$ material. [30] Further, many literatures have explored the use of differential voltage analysis (DVA) to study aging. One such study, Lewerenz et al, uses DVA for calendar and cyclic aging of cylindrical LFPC cells and focusses on mechanisms of homogeneity of active lithium distribution and loss of active anode material. They arrive at the conclusion that degradation during cyclic aging can be due to different phenomena, such as loss active lithium, local loss of active anode material for depth of discharge (DOD) 100%, deactivation of certain layers of anode and cathode due to a lithium-permeable covering layer on top of the anode. [31]

The literature reviewed for the aging revealed many different trends for different cells. Despite that, not much work has been done for the distinction of aging among lithium-ion cells based on packaging geometries (cylindrical cells being the most popular geometry for research). But the different mechanisms of aging have been well researched and as discussed above can be mainly categorized as loss of lithium inventory (LLI), loss of active material (LAM), ohmic resistance increase (ORI) and lithium plating. As discussed in the next paragraphs, these mechanisms are interrelated and are tailored around the SEI layer formation and disruptions in it. The next subsection briefly discusses the concept of SEI layer formation, its importance for the cell aging and the different aging mechanisms.

In this thesis, the effects of high and low temperatures, and high currents on the aging have also been considered. Uddin et al. [32] have summarized all the possible effects of these conditions on the cells and the results are summarized using the flowcharts in

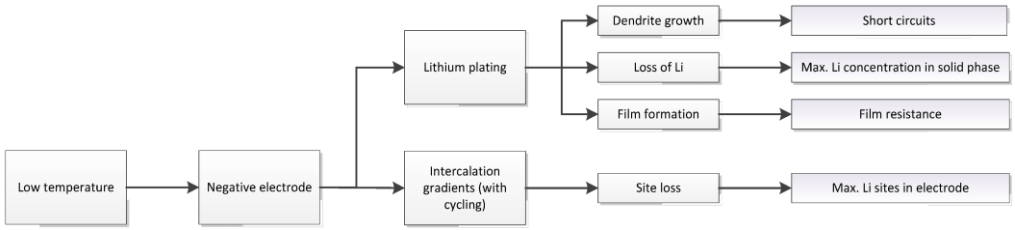

(a)

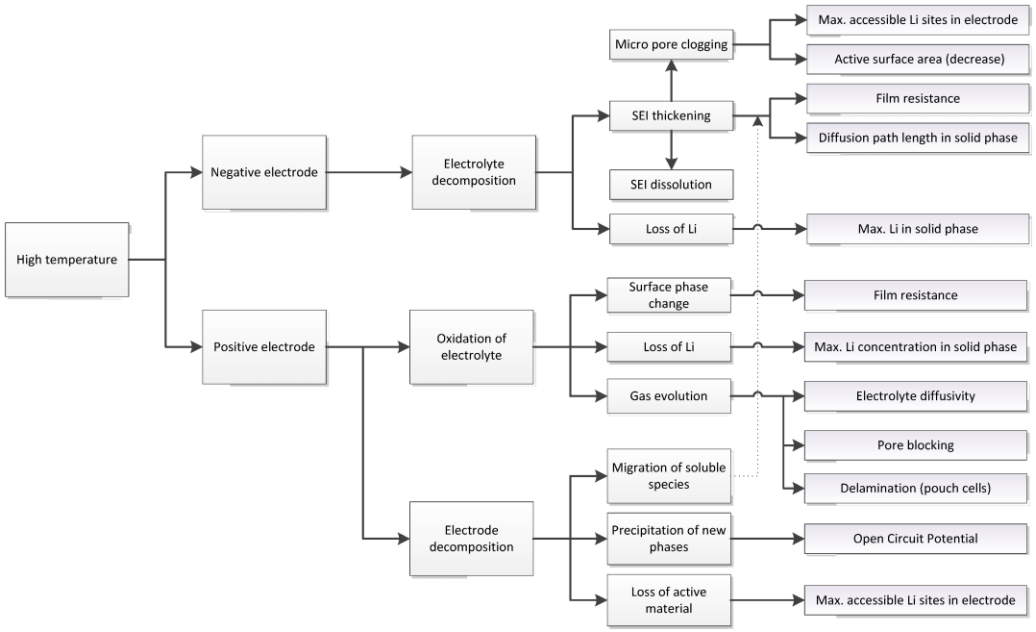

(b)

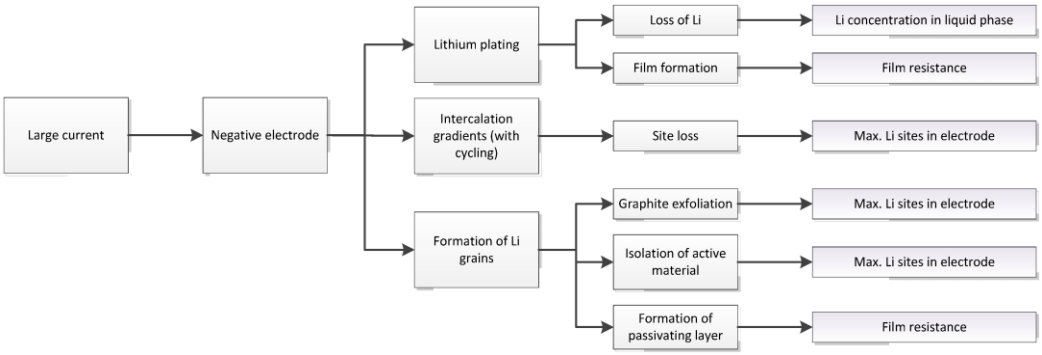

(c)

Figure 3.1. Battery degradation due to cycling at (a) low temperature, (b) high temperature, (c) large currents [32]

3.2.1 SEI layer formation

During the first charging cycle of a lithium-ion cell, a passivation film builds on graphite/electrolyte interface. When the charging process starts, Li^+ ions travel through the electrolyte towards the graphite anode. Some Li^+ ions react with the degradation products of the electrolyte and form insoluble parts that deposit on the anode. Slow charging results in densely packed SEI layer which prevents graphite structure from decomposition. Then the SEI layer strips off the solvent molecules surrounding the Li^+ ions. Additionally, the SEI layer prevents the anode lattice from exfoliation and in an ideal case, allows cycling of lithium batteries without major capacity fades (except for the initial capacity drop loss due to losing lithium inventory to SEI layer formation). [33] It is vital to the performance of the lithium-ion cell, since the entirety of the anode must have a uniform layer of SEI to prevent further disintegration of the electrolyte. [20]

Xu [34] has performed a review of the chemistry involved in non-aqueous electrolytes in lithium-ion batteries and also included a detailed description of passivation layers and SEI layer formation. It first explains passivation as the process where the products from the initial decomposition of electrolyte form a dense, protective film that covers up the pristine surface of the electrode and prevents any sustained decompositions. He also concludes from a study of other works that these passivation layers are the foundation upon which lithium-ion batteries are built. The work further goes on to discuss the formation of passivation layers on both the cathode and the anode. For simplicity of discussion, it is the passivation layer formed on the graphitic anodic layer which is widely regarded as the solid electrolyte interface layer (SEI). The study on this SEI layer on graphite is more advanced and the effects due to any changes in it are more pronounced. Xu further argues that the formation of the SEI layer is what makes the reaction within the cell reversible, by preventing consumption of both the electrolyte and more active lithium. This SEI layer is an ionic conductor and electronic insulator. [34]

The SEI layer is a mix of lithium oxide, lithium fluoride and semi-carbonates (lithium alkyl carbonates). A schematic of the SEI layer formation as illustrated by Xu is shown in Figure 3.2. Upon cathodic polarization of the graphite anode, the solvated Lithium-ion migrates to the negatively charged surface of graphite and is intercalated into graphene layers before any reduction occurs. The ternary graphite intercalated compound (GIC) thus formed has a short lifetime and decomposes within the time scale of slow scan cyclic voltammetry, a process that might easily be mistaken as an ordinary irreversible reduction of the electrolyte. However, at certain faster scan rates, part of the solvated ion could still be reversibly removed from graphene interlayer sites. The reductive decomposition of these co-intercalated

solvents then renders an SEI that extends from the graphite surface at the edge sites into the interior of the interlayer voids. [34]

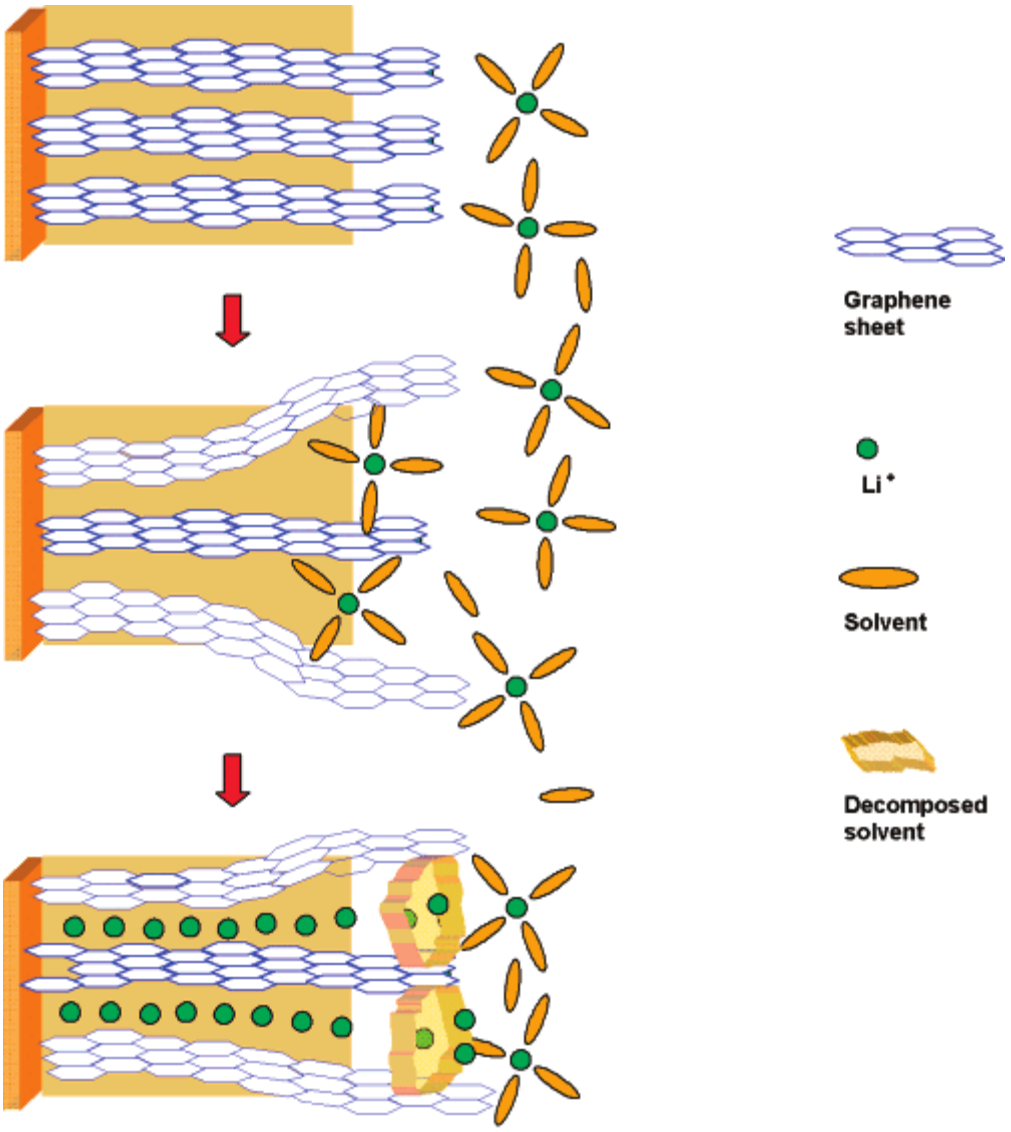

Figure 3.2. Schematic illustration of SEI layer formation [34]

An optimized SEI layer is expected to have negligible electrical conductivity, high electrolyte diffusion resistance while having high lithium selectivity and permeability. Once it is properly formed, further decomposition reactions with salts and solvents are prevented as electrons cannot transfer to or through the layers. Properties of an ideal SEI formation are high electrical resistance, high lithium selectivity, high strength, tolerance to expansion and contraction stresses. [20] It should also have zero electron transference (to avoid tunneling), high ion conductivity, uniform morphology, good adhesion to carbonaceous anode surface, mechanical strength and flexibility, and low solubility in electrolytes. [34]

In real cases, the SEI-layer thickens gradually by repeated cycling due to electron exposure to electrolyte and electrolyte diffusion to graphite surface. Various factors can lead to further irreversible SEI layer formation consuming both electrolytes and active lithium. For example, SEI has been found to be damaged at elevated storage temperatures by the successful detection of reappearance of the irreversible process at 0.75V. [34] This not only leads to electrolyte decomposition but also might lead to loss of active lithium. [20] The most common and fundamental source of capacity fade in successful lithium-ion batteries (which manage to resist degradation over hundreds of cycles) is the loss of lithium to the SEI, which typically forms at the negative electrode during recharging. [27] Four different aging mechanisms attempt to explain various ways in which this can happen.

3.2.2 Aging mechanisms

Four major aging mechanisms are studied by most literatures to account for the capacity fade in lithium-ion batteries which are: loss of lithium inventory (LLI), loss of active material (LAM), ohmic resistance increase (ORI) and lithium plating. Often these mechanisms are inter-related as discussed in this section.

Loss of lithium inventory (LLI) leads to loss of lithium ions due to parasitic reactions, though it does not change the content of active materials in electrodes and their properties. It is reported to be the major cause of degradation of lithium-ion batteries. It is attributed to two main causes: the primary cause is the SEI layer formation, growth and destabilization, and the secondary cause is the side reactions of lithium-ion with decomposed electrolyte compounds and water in the electrolyte. LLI occurs chiefly at the electrode/electrolyte interface and is predominant on the negative electrode where SEI formation dominates. SEI growth and subsequent LLI is dependent on temperature. At high temperatures, the SEI either grows in thickness or becomes non-protective leading to performance degradation, whereas at low temperatures, the risk of lithium plating leads to cell degradation. [24]

Loss of active material (LAM) directly affects the structure of the electrodes, reducing the volume of active material used in the cell. The aging effects due to LAM are more prominent in graphite based negative electrodes than positive electrodes. It is enhanced by high currents, high temperatures and high SOC. The major reasons of LAM are: particle isolation, side reactions within the active material of the electrodes and physical degradation. LAM may lead to second stages of cell degradation where abrupt capacity losses might appear after steady capacity loss in the first stage. [24]

In ohmic resistance increase (ORI), degradation caused on the electrodes and electrolyte materials directly result in the increase in the electronic and ionic resistances, respectively. The possible reasons for ORI are particle isolation causing LAM, binder decomposition, current collector corrosion, volume changes in active material and electrolyte contamination, and SEI growth and destabilization affecting ionic resistance. [24]

Lithium plating occurs during charging when Li ions deposit on the negative electrode instead of intercalating into the graphite. It is the most detrimental aging mechanism as it also leads to safety deterioration. It can result from large number of factors, like constructive properties of the cell to operating conditions (like low operating temperatures and high current rates). Lithium plating increase LAM and LLI. It is initiated by strenuous charges, charging at low temperatures, cell constructive design or conventional aging of the cell. [24]

One of the major consequence of aging is the changes in the internal resistance of the cell, mostly an increase, and the next subsection studies the overpotentials and the internal resistances involved.

3.2.3 Internal resistances and overpotential

In this thesis, the internal resistance has been measured through 30s pulse (charging and discharging test) which will be further discussed in the next chapter. The purpose of the pulse tests is to separate the resistances associated with different electrochemical processes during cycling at different state of charge (SOC) of the cells. This sub-section includes a literature review of the different attempts at separating the resistances based on ohmic resistances and different overpotentials or polarization. It also includes a study of factors contributing to the resistances and the different kinds of internal resistances. Finally, an educated approximation is made to study the internal resistances and polarization in this thesis.

Polarization curves are a popular way to study the behavior of a cell during operation. DuBeshter [35] has discussed a way to develop pulse polarization curves (PPC) for a Lithium-ion battery under constant SOC to identify individual over-voltages, such as charge transfer kinetics and mass transport, and their SOC dependence. In this work, different time scales of a discharge pulse have been formulated to represent the kinetic overpotential, electrolyte Li^+ concentration and Li solid state diffusion.

Liu et al. [36] have studied the differences in electrochemical potentials in different rechargeable batteries. Lithium-ion batteries are always accompanied by solid-state mass diffusion as well as volume expansion or contraction, although the electrode surfaces do not recede

or advance when the volume change of electrodes is not considered. While the concentration of Li ions remains constant in the electrolyte regardless of the degree of charge or discharge, it varies in the cathode and anode with the charge and discharge states. Liu et al.[36] further summarize that an SEI film permits the diffusion of Li ions through the film under a uniform electric field and reduces the overpotential and concentration polarization. The SEI can also prevent the aggregation of electrochemically active particles and maintain a uniform chemical composition at the electrodes. The SEI film increases the internal resistance of the battery and consumes part of the lithium ions from the cathode, leading to both power and capacity loss. This helps in correlating the SEI film formation with the polarization process, internal resistance increases and capacity losses.

Saha and Goebel [7] have done a study on the modeling of lithium-ion battery capacity depletion in a particle filtering framework and have further described the battery characteristics and the concept of overpotential in their work. Park et al. [37] have done a review of the conduction phenomena in lithium-ion batteries and have explained the term polarization curve. The cell potential is calculated as the difference of the Gibbs free energies the product of the reactants and products (potential difference between the electrodes), with the theoretical open circuit voltage, E^o, measured with the reactants at 25°C and 1M solutions. This is the equilibrium potential. But during the operation of the battery, due to current flow or charge flow, the potential deviates from the equilibrium and this shift is known as the polarization. In the case of oxidation (loss of electrons), the actual potential is more than the equilibrium potential, while the vice-versa is true for reduction (gain of electrons). This shift or voltage drop is due to various passive components inside the electrolyte, the separator, the terminal leads etc., which are characterized by the following factors [7]:

- Internal resistance (IR) drop: Voltage drop associated with the internal resistance of the battery during the current flow across the terminals. The internal resistance has been categorically divided in Table 3.1.
- Activation polarization: This involves the kinetics involved with the electrochemical reaction, for e.g., work function that the ions must overcome at the junction between the electrodes and electrolytes. It is associated with the kinetics of charge transfer.
- Concentration polarization: The potential drop associated with the mass transfer resistance (e.g. diffusion) during the ion transportation across the electrolyte from one electrode to another. It is associated with the kinetics of mass transfer.

This can be mathematically denoted using the equation

(3.1) [7]:

$$E = E_0 - [(\phi_{ct})_a + (\phi_{ct})_c] - [(\phi_c)_a + (\phi_c)_c] - iR_i = iR \quad (3.1)$$

where, E_0 is the standard cell potential, $(\phi_{ct})_a$, $(\phi_{ct})_c$ are activation polarizations (charge-transfer over voltage) at the anode and cathode, $(\phi_c)_a, (\phi_c)_c$ are concentration polarizations at the anode and cathode, i is the cell operating current, R_i is the internal resistance of the cell and R is the apparent cell resistance.

Zhang Zhou et al. [38] have studied different dynamic phenomena inside the battery: lithium-ion migration through the solid electrolyte interface (SEI) layer, activation kinetics in both negative and positive electrodes, double layer effects at the interfaces of electrolytes, and lithium-ion diffusion processes in the active material of the electrodes. They also discussed the overpotentials and resistances related to the various sections of the reaction cell by performing the electrochemical impedance spectroscopy (EIS). This can be explained using the Figure 3.3. The different regions correspond to different internal resistances and chemical phenomena. Region A can be represented by single ohmic resistance, R_o, and includes resistances of the current collector, active material, electrolyte and separator. Region B represents the SEI layer resistance (R_{sei}) – characterized by a high frequency. Region C (medium frequency) represents the charge transfer resistance (R_{ct}). The low frequency region, D, represents the lithium-ion diffusion process in the active material of the electrodes. [38]

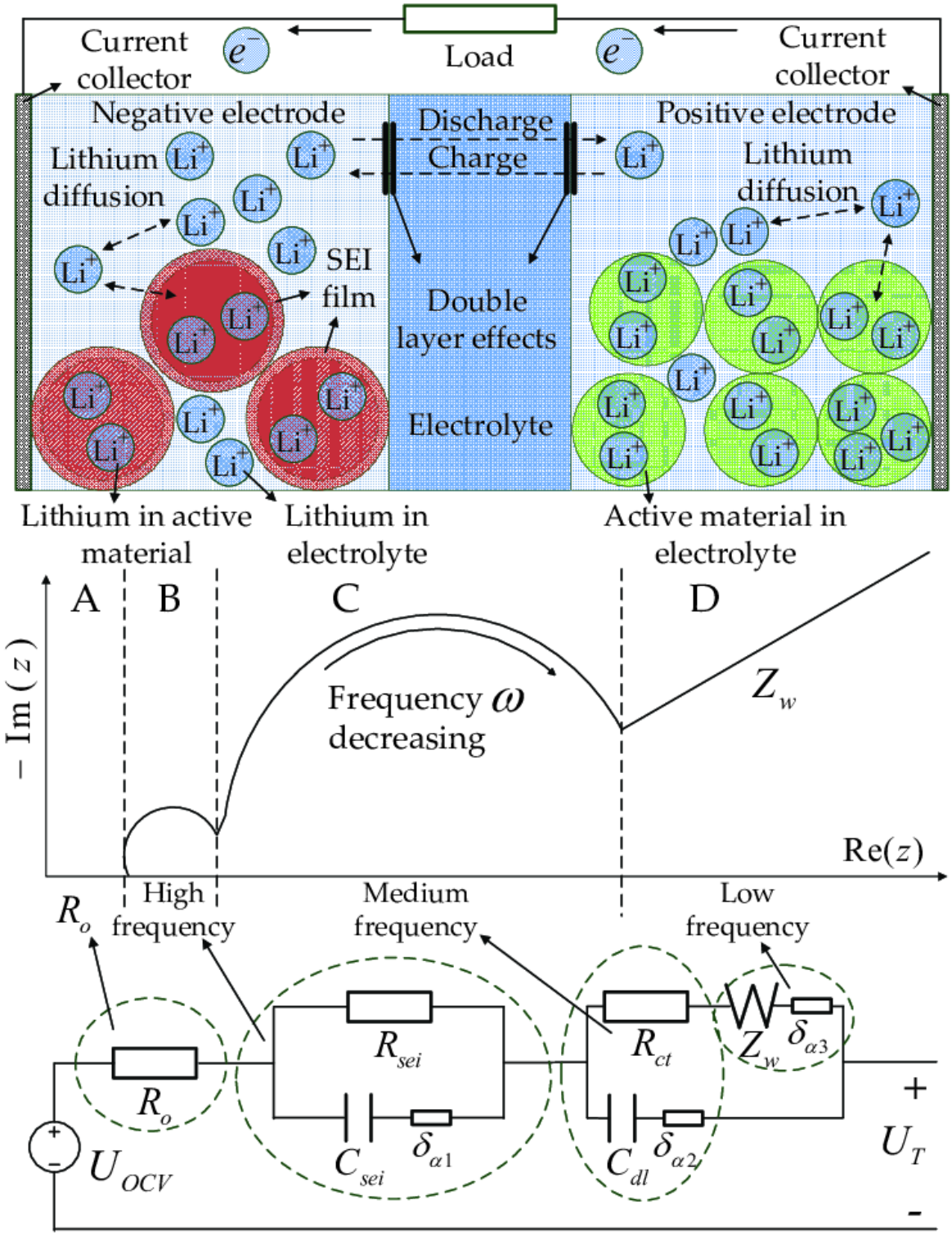

Figure 3.3. Lithium-ion cell internal dynamics and equivalent impedance circuit. [38]

The internal resistance of a cell as studied from the literature review above can be summarized as shown in Table 3.1 below:

Table 3.1.Types of internal resistances [37]

Type of resistance	**Internal resistance of cell, R_i=ionic resistance + electrical resistance + interfacial resistance**
Ionic	• Electrode particle • Electrolyte
Electrical	• Electrode particle • Conductive additives • Percolation network of additives in electrode • Current collectors • Electrical taps
Interfacial	• Between electrolyte and electrodes • Between electrode particles and conductive additives • Between electrode and current collectors • Between conductive additives and current collectors

Further, Park et al.[37] have reviewed the electrical and ionic conductivity separately for anodes and cathodes, especially with interesting insights into $LiFePO_4$ based cells. Assuming diffusion governs charge/discharge rates, ionic conductivity is more significant than electronic conductivity because high ionic conductivity will allow rapid diffusion of Li ions into the cathode materials in the case of charging. Conduction in graphite anodes is complex due to the continuous phase transformations and the formation of SEI layers. A prominent feature of graphite anodes is the staged intercalation of lithium-ion, and the diffusivity of Li ions in graphite is found to be a function of intercalation or electrical voltage. [37] It is concluded that major features of conduction in the anode are closely related to phase transformations as a function of lithium-ion intercalation and SEI layer formation.

In order to locate the different regions of a polarization curve based on the cell chemistry, DuBeshter and Jorne [35] have designed a method to adapt polarization curve from fuel cells to lithium-ion batteries in order to understand the governing factors of battery performance under various operating conditions at different SOCs The polarization curve here can be divided into three parts, namely, (a) the activation part representing the kinetic region, (b) the ohmic part representing the ionic exchange, and (c) the concentration part representing the mass-transfer region. The adapted method can be used to give information about the charge transfer kinetics, ionic mass transport and solid-state diffusion. According to this method, for the pulse test, different time instants of the pulse represent different parts of the three governing factors. To create pulse polarization curve using this method, the end SOC must remain constant and that is the reason why the pulse test in this thesis is performed at a constant SOC.

DuBeshter and Jorne [35] performed pulse discharge experiments and partially separated the charge transfer kinetics, Li^+ ionic mass transport and Li-solid state diffusion losses by utilizing different pulse discharge times and examining the relaxation curves. They separated the overpotentials as mentioned by separating time scales for the pulses using the equation (3.2) given below [35]:

$$\tau_s = \frac{L^2}{D} \tag{3.2}$$

where, τ_s refers to the time scale, L is the characteristic length, D is the diffusion coefficient. Following experiments and calculation based on this equation, they made certain observations regarding the cell overpotentials. Voltage losses related to the kinetics occur in the order of 1ms (length in equation (3.2) derived from SEI thickness and diffusivity related to electrode active solid particles). At the 2s instant, the charge transfer kinetic losses are governed by intercalation/de-intercalation of Li^+ ions at the interface of the electrode active materials. The Li+ concentration gradient formation characteristic time is found to be about 5 to 10s (based on electrode and separator thicknesses, and diffusivity of the electrolyte). While by a pulse length of 10s, it is assumed that the concentration gradient of the Li^+ ions is fully formed within the electrolyte of the battery, but the solid-state diffusion has not changed significantly. The characteristic time for Li diffusion into the electrodes is found for the cells tested by them to be about 20-200s (based on half-cell diffusivity and measured solid particle radii). Therefore, the 30s pulse instant is deduced to correspond to the lithium-ion diffusion in the electrode's active materials. [35]

The works of Zhang Zhou et al. [38] and DuBeshter and Jorne [35] are in support of each other. The high frequency or the early time instants of a pulse correspond to the charge transfer kinetics, the medium frequency region or mid time instants represent the formation of the Li^+-electrolyte concentration gradient formation and the low frequency regions or later time instants represent lithium-ion diffusion process in the active material of the electrodes. Resonating these works, Barai et al. [39] have studied the effect of measurement time-scales on DC internal resistance measurement. Figure 3.4 shows a schematic of a cell voltage response to a pulse current. Based on the time scales, the voltage drop phenomena can be differentiated as [39]:

- the instantaneous voltage drop is due to the pure ohmic resistance (R_o) which comprises all electronic resistances and the bulk electrolyte ionic resistance of the battery
- the potential drop within the first few seconds is due to the battery's double layer capacitance and charge transfer resistance (R_{ct}) which is attributed to the charge transfer reaction at the electrode/electrolyte interface
- the shallow, linear (or close to linear) voltage drop is due to polarization resistance (R_p) which accounts for ionic diffusion in the solid phase and is usually considered to be the rate determining step for Li ion batteries

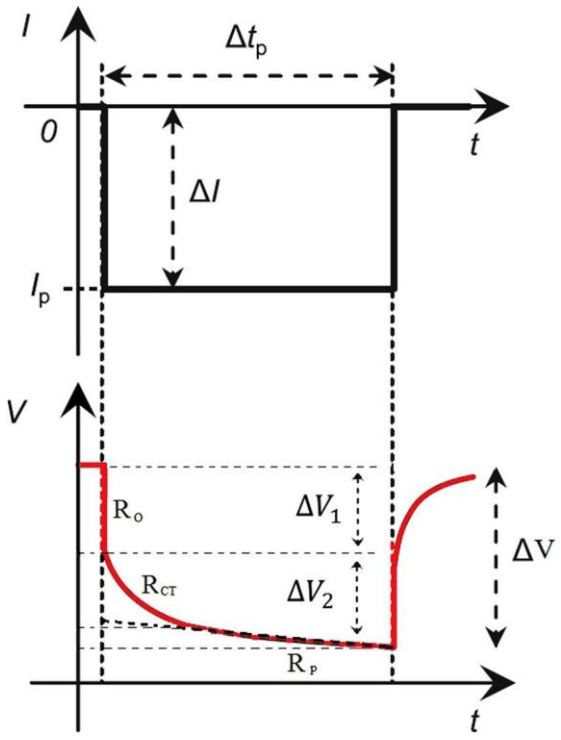

Figure 3.4. Schematic to show cell voltage response to a pulse current. [39]

The approximation done by Barrai et al. will be used to study the 30s pulse test in this thesis. To understand these phenomena, the charge-discharge process of lithium-ion cells is

discussed in further detail. The cell electrochemical behavior is usually modeled with respect to various parameters like electrolyte concentration, electrolyte potential, solid-state potential, and solid-state concentration in the porous electrodes and electrolyte concentration and electrolyte potential in the separator. These models are based on transport phenomena, electrochemistry, and thermodynamics.

3.2.4 Cell Electrochemistry

Jow et al. [40] [41] have discussed the Li^+ charge transfer process and the charge-discharge kinetics in detailed. During charging, at the positive electrode side, a dissolution takes place between the positive electrode (cathode) and the passivation layer formed on the cathode, producing Li^+ and an electron. The electron travels across the electron conducting network within the electrode and reaches the current electrode at the outside. The Li^+ is then transported to the negative electrode, in a solvated form (shown as "Li^+" in equation (3.4)). Next, at the negative electrode (anode), the de-solvation of this ion takes place whereby the "Li^+" sheds the solvated solvent molecules before transporting through the SEI (on the anode surface). At the anode, the Li^+ takes an electron and intercalates into the anode surface. This whole process of charging is explained using the equations below [40]:

At the cathode,

- Li de-intercalation, dissolution from $LiFePO_4$ to become Li^+ and e^-

$$LiFePO_4 \rightarrow x\,Li^+ + x\,e^- + Li_{1-x}FePO_4 \tag{3.3}$$

- Li^+ transport through the passivation layer on cathode.
- Li^+ solvation in the electrolyte

$$Li^+ \rightarrow "Li^+" \tag{3.4}$$

At the anode,

- De-solvation of the "Li^+" at the SEI/electrolyte interface

$$"Li^+" \rightarrow Li^+ \tag{3.5}$$

- Li^+ transport through the SEI towards anode
- Li^+ reaching the anode and accepting an electron at the anode-SEI interface.

$$xLi^+ + xe^- + C_6 \rightarrow Li_xC_6 \quad (3.6)$$

During the discharge process, the steps are reversed. Jow et al. also noted that the de-solvation process (equation (3.5) above) is the predominant limiting factor. [41] Figure 3.5 illustrates the charge transfer during charging and discharging.

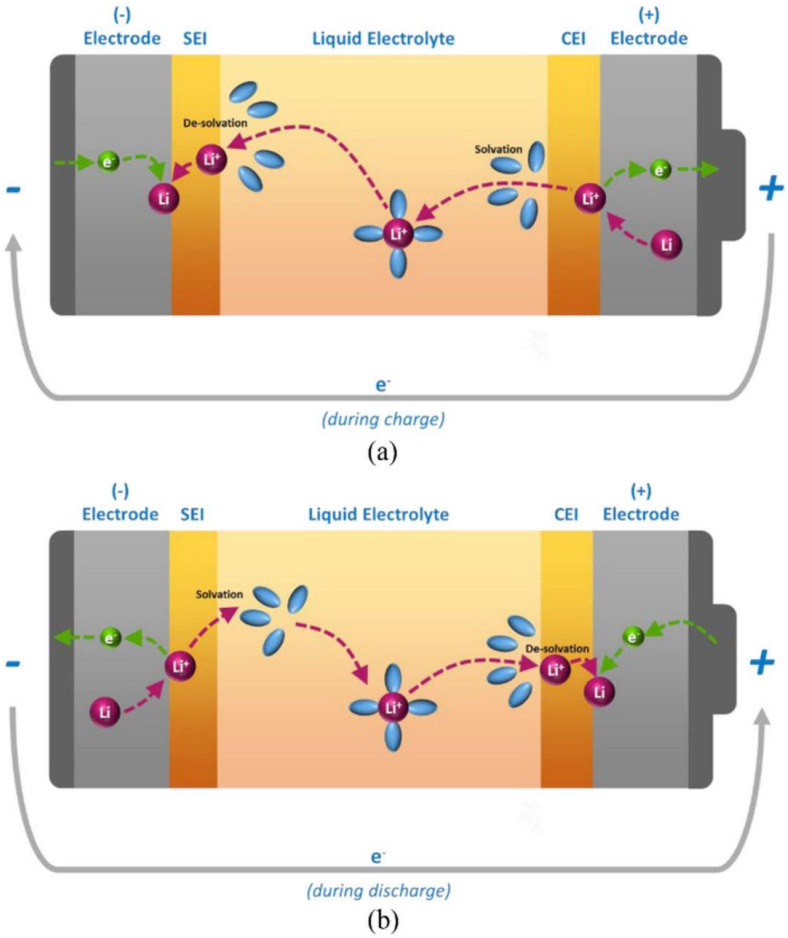

Figure 3.5. Charge transfer kinetics mechanism during (a) charge and (b) discharge [40]

In the initial stages of charging or discharging, the electrical or ohmic resistances dominate, while ionic or polarization resistances take over when the process continues. Polarization is the potential gradients developed as described in previous sections. These show up at different stages of a pulse test (as described earlier in this sub-section), as they take different time durations to form. One such process is the formation of a concentration gradient in the presence of an electrolyte with a non-unity transport number, due to limitations in ion transport. [42] [43] The properties that determine how fast this gradient is formed are: diffusion coefficient, transport number and thermodynamic enhancement number. The diffusion

coefficient is usually determined based on electrolyte salt concentration gradients. The transport number is a measure of the fraction of the current being carried by the lithium-ion. The thermodynamic enhancement factor is a measure of how the thermodynamic driving force relates to concentration gradients and depends on the activity coefficient. [43] It is understood that the mass transport concentration gradient is dependent on the chemical nature of the electrolyte.

Lithium-ion diffusion, on the other hand, in the active electrode material is directly related to the power density. The lithium-ion diffusion into and out of the electrode active material (intercalation and de-intercalation) is modeled using Fick's law of diffusion. $LiFePO_4$ have less lithium-ion diffusivity as compared to other cathode chemistries and therefore, is often doped with carbon. In addition to the chemical diffusion coefficient, the lithium diffusion depends on factors like porosity and tortuosity. Porosity is the measure of the void fraction within the electrode structure into which the lithium-ion can intercalate. Tortuosity is a term used with porous particles to describe the efficiency of the percolation path and is related to the topology of the material. Figure 3.6 below shows a typical porous electrode in lithium-ion cells. During charging, the Li leaves the structure of $LiFePO_4$ and intercalates into the porous graphitic structure of the anode, while during discharge, it de-intercalates from the anode to remix with the cathode structure.

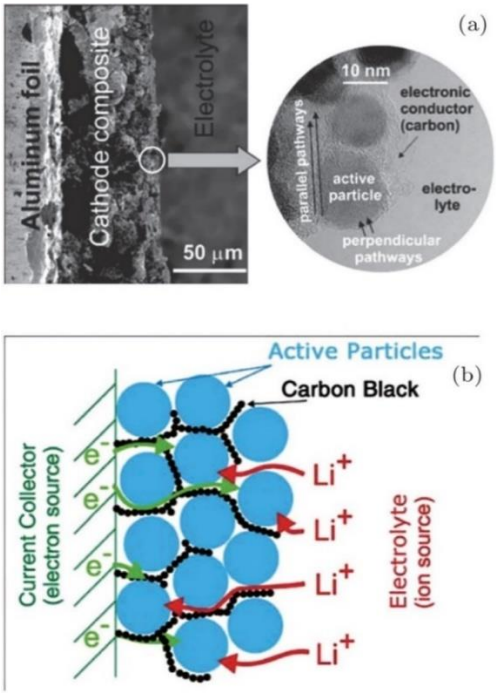

Figure 3.6. The porous electrode of a Lithium-ion battery (a) Low magnification (on left) and high magnification (inset on the right). (b) Schematics showing the main phases constituting a modern insertion cathode and its role in transport. [44]

The electrochemical behavior of the cells in this thesis are discussed using the DC pulse test, where the measured internal resistances refer to the electronic and ionic resistances as separated in this section. For secondary or rechargeable cells like lithium-ion cells, these parameters differ greatly from one SOC value to other (i.e. the capacity contained in the cell at that instant), therefore, the pulse test is done for different SOCs. A drawback of using DC current to obtain resistances is that it shows only the imposition of all the different contributions to resistance, hence there is an inability to completely separate the different resistance components. [39]

This chapter served to understand the underlying theory behind the work done in the thesis. A literature review of the studies on packaging geometries was followed by a summary of the cell aging mechanisms. Further, the methods to classify resistances and polarization based on the chronological electrochemical processes were studied and a adapted for the thesis work. The next chapter discusses the specifics of the cells manufactured and moves on to the experiments performed on the cells within the scope of the thesis.

4 Experiment

This chapter discusses the conditions and methods for the manufacture of the cells along with the cell testing. In the first part, the cell geometry, size and chemical composition of the cathodes and anodes are mentioned. The second part describes the test performed on the cells which are used within the scope of this thesis.

4.1 Cell chemistry

To have a common comparison standard between the cell packaging geometries, the chemistry for the anode, cathode, electrolyte and separator were chosen to be the same. All cells manufactured have the same materials for the electrodes, i.e., $LiFePO_4$ as the cathode and graphite as the anode. Both the materials of the electrodes are from the same batch of raw materials for all the cells. [45]

The separator used for the cell manufacture is a tri-layers Celgard 2325 grade. This type of tri-layered poly-olefin separator consists of 1 polyethylene (PE) layer sandwiched between two layers of polypropylene (PP) and is the most commonly used separator type. This is because of their chemical inertia and the safety feature the combination of PP-PE-PP offers. In the case of overheating, the PE layer melts, losing its porosity (i.e., mechanically blocking the Li^+ ion movement), while the PP layer prevents large dimensional changes until its own melting, thus preventing short-circuits.

The composition of the electrolyte solution strongly influences the temperature dependence of the capacity. This is related to the quality of the passivation of the graphite electrodes in the various solutions and to the transport properties of the passivating surface films that cover the graphite particles (discussion related to SEI layer formation). [46] For the cells manufactured by SPICY, the electrolyte solution used is a blend of ethylene carbonate (EC), propylene carbonate (PC) and di-methyl carbonate (DMC) in volume proportion 1:1:3, respectively, with 1M of LiPF6 and 2% weight of vinylene carbonate (VC). [45]

4.2 Cell geometry and size

The three packaging geometries (cylindrical, prismatic and pouch) were assembled in different ways, which are mentioned in the SPICY Deliverable 5.6.

Jelly roll manufacturing was used to wind together the electrodes and separator in cylindrical and flat cores ***for cylindrical and prismatic cells***, respectively. While the cylindrical cores are basically rolls of electrodes with separators within them, for the prismatic cells, the cores resemble layers placed into a Z-shape. Next, the cells are welded together complete with the placing the current collectors and finally welding the top cap. The electrolyte is filled using different holders through the aperture at the top cap. It is necessary to ensure that the electrolyte solution covers every pore in the internal structure and the separator membrane. After this step, the cells are conditioned outside the dry room.

The ***pouch cells*** were manufactured separately. The process lacked a standardized equipment and therefore, needed a lot of workforce and manual job initially. In the first step, the electrodes and the separators were cut into layers using a cutting press and stacked into layers of 38 anodes, 76 separators and 37 cathodes. The terminals were drawn out and tabs were welded on them. The stacks thus formed were wrapped in two half-aluminum shells and heat sealed. The pouch cells were filled with the electrolyte solution in a glove box and the remaining side was welded. Then the cells were conditioned outside the dry room and the trapped gas bubbles in the structure were degassed as the last step. The three cell geometries manufactured are shown in Figure 4.1.

(a) (b)

Figure 4.1. Cells manufactured (a) Prismatic (L), Cylindrical (R), (b) Pouch [45]

The post manufacturing specifications of the cells are reported further in this sub-section. The cell specifications of each geometry are mentioned in the Table 4.1.

Table 4.1. Cell specification for cells of different geometries [44]

	Cylindrical	**Prismatic**	**Pouch**
Lower Voltage limit (V)	2.5	2.5	2.5
Upper Voltage limit (V)	3.6	3.6	3.6
Max charge current (A)	50	4	50
Max discharge current (A)	100[1]	4[2]	100[3]
Temperature range (°C)	[-10, +55][4]	[0, +45]	[-10, +55][5]
Energy density (Wh/kg)[6]	108.61	94.25	121.77
Capacity (Ah)	16.099	15.963	14.889
Weight (g)	474.32	541.98	391.25
Height (mm)	125	125	-
Surface area (mm²)	19625[7]	31250[8]	-

[1] for a 30s pulse

[2] normal cycling, rate tests upto 12A

[3] for a 30s pulse

[4] for charging [+5, +55]

[5] for charging [+5, +55]

[6] Energy density, $E = \frac{Q \times V_{nom}}{m}$, where Q = Capacity, V_{nom} = nominal voltage, m = mass

[7] Curved surface area of cylindrical cell = $2\pi rh$

[8] Curved surface area of prismatic cell, considered to be cuboidal = $2(l + b)h$

A weight analysis was done for all the cells and the average weight contribution of the different components of each cell are shown in Figure 4.2. A clear difference is noticed in the cells with soft packaging, i.e. the pouch cells, due to softer casing.

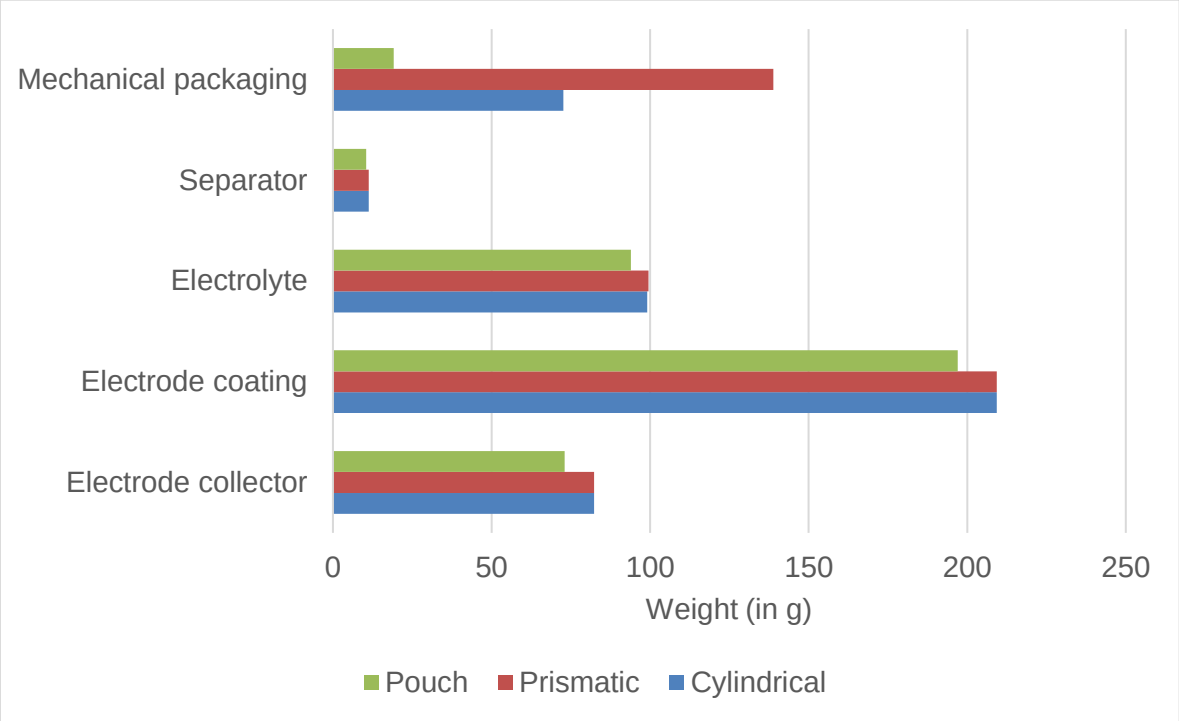

Figure 4.2. Weight analysis of the cells. [45]

The weight analysis is as expected because of the hard cover being replaced by aluminum foil in the pouch cells, reducing the weight of the packaging component. In the case of the prismatic cell, it requires more packaging than a cylindrical cell because of the higher surface area, as can be seen from the reception test data given in Table 4.1.

The data presented above were measured without any aging. After the reception tests, the cells were aged and cycled at different stages of State of Health (SOH). The following subsection explains the different tests performed relevant to the current work.

4.3 Tests performed

Within the scope this thesis, only the life cycling tests have been included. It involves testing of the cells at different charging/discharging rates at different conditions of temperature over different states of health (SOH) or aging time. In the cycle tests, the equivalent full cycles are observed over the aging of the cells.

All the cyclic life tests involve two kinds of checks – short check-up (SCU) and extended check-up (ECU). The extended check-ups (ECUs) involve the measurements of capacity evolution, open circuit voltages (OCV) and internal resistances by pulse tests. Another test

involves the temperature developed at the first ECU for different charging and discharging rates. Within the scope of this thesis, the capacity evolution, the internal resistance developed at different capacities (pulse tests) and the temperature are the most interesting.

The tests were carried out using the Extended Cell Test System (XCTS) provided by BaSyTec GmbH. According to the BaSyTec XCTS product brochure, this lithium-ion cell formation and test system has current capabilities up to 25A or 50A. It has the advantage of low working expenses because of the option of energy recovery heat generation. Using the 50A system, currents up to 300A can be produced using parallel operation facility. The system control is done using the high speed and precision BaSyTest software. Due to such features, this system finds application in test of large lithium-ion cells, high power tests, pulse tests and formation of lithium-ion cells.

The life-cycle test standards are documented in Spicy Deliverable 6.1. The usual test conditions as mentioned in this deliverable can be enumerated as follows [47]:

i. The state of charge calculated is the capacity calculated at usual discharge rate of 1C at 25°C.
ii. The state of health (SOH) refers only to the battery capacity decrease.
iii. The usual test conditions of C-rates for charging are 1C, 2C, whereas for discharging are 0.2C, 0.5C, 1C, 2C
iv. For this work, the SOC window for cycling is 0% to 100%
v. The end of life (EOL) is set to 80% of initial capacity and most test results in this work contains values for a minimum SOC around 80%.

The following sub-sections cover the tests performed on the cells which are relevant within the course of the work.

4.3.1 Capacity evolution of the cells

This test is performed to determine the cell deterioration or capacity loss. Of special interest is the capacity deterioration over the possible number of equivalent full cycles (EFC). The capacity deterioration is measured as SOH drop.

As mentioned earlier in the discussion of the test conditions, the state of health (SOH) refers only to the battery capacity decrease. The SOH is not a well-defined physical quantity. It can be defined and determined by using any measurable quantity that changes with aging of the cell for example capacity, internal resistance, cell impedance, cycling temperature gradient changes etc., and is monitored with respect to the values for a new cell. Therefore, such details are not provided by the manufacturers and must be independently determined by the

testing infrastructure. There is no precise definition of SOH agreed upon uniformly by industries or scientists [48]. The SOH estimation within this work, as mentioned, has been done by measuring changes in the capacity of a fully charged cell. It can be depicted using the equation (4.1) [48]:

$$SOH = 1 - \frac{Q_{full,aged}}{Q_{full,new}} \tag{4.1}$$

Here, $Q_{full,aged}$ refers to the capacity of the aged (current state) cell at full charge (i.e. at an SOC of 100%), while, $Q_{full,new}$ refers to the capacity of a new unaged battery at 100% SOC. There are many different methods to calculate the capacity of the cell, for e.g. coulomb counting and open circuit voltage method [48].

For this work, the charge-discharge cycling method and the subsequent SOH calculation is described below with the help of Figure 4.3. The figure shows a sample plot taken from a test on a cylindrical cylinder. It shows the instantaneous capacity and the current profiles for charging and discharging. It helps to show how the SOH is being calculated. The cells were charged and discharged using the conventional constant current – constant voltage (CC+CV) and constant voltage (CV) protocols. [49] The CC+CV protocol is the most popular charging procedure for lithium-ion batteries. It involves a low rate constant current charging to a predefined cut-off voltage followed by float charging at the cut-off voltage until the current drops to very low preset value. The positive current and instantaneous capacities are for charging, while the negative values depict discharging.

i. An unaged cell is fully discharged, and the residual capacity is measured and noted.
ii. Next the cell is charged again first with constant current (CC) and then with constant current + constant voltage (CC+CV). When the cell is fully charged, the capacity is measured again and noted.
iii. This fully charged cell is discharged again and another discharge cycle, as described in step ii above, is carried out.
iv. The cell is charged a second time and the cell capacity after the second discharge is noted and labelled as the $Cap_{reference}$ (reference initial capacity) of the unaged cell. This corresponds to the capacity at 100% SOH.
v. Steps i through iv are repeated for the aged cell and the cell capacity after the second discharge-charging cycle is noted and saved as $Cap_{i,aged}$ (the capacity

of the aged cell at the i[th] step). The SOH of the aged cell is calculated using the equation

vi. (4.2):

$$SOH_i = \frac{Cap_{i,aged}}{Cap_{reference}} \times 100 \quad (4.2)$$

where, SOH_i is the state of health at the i[th] step

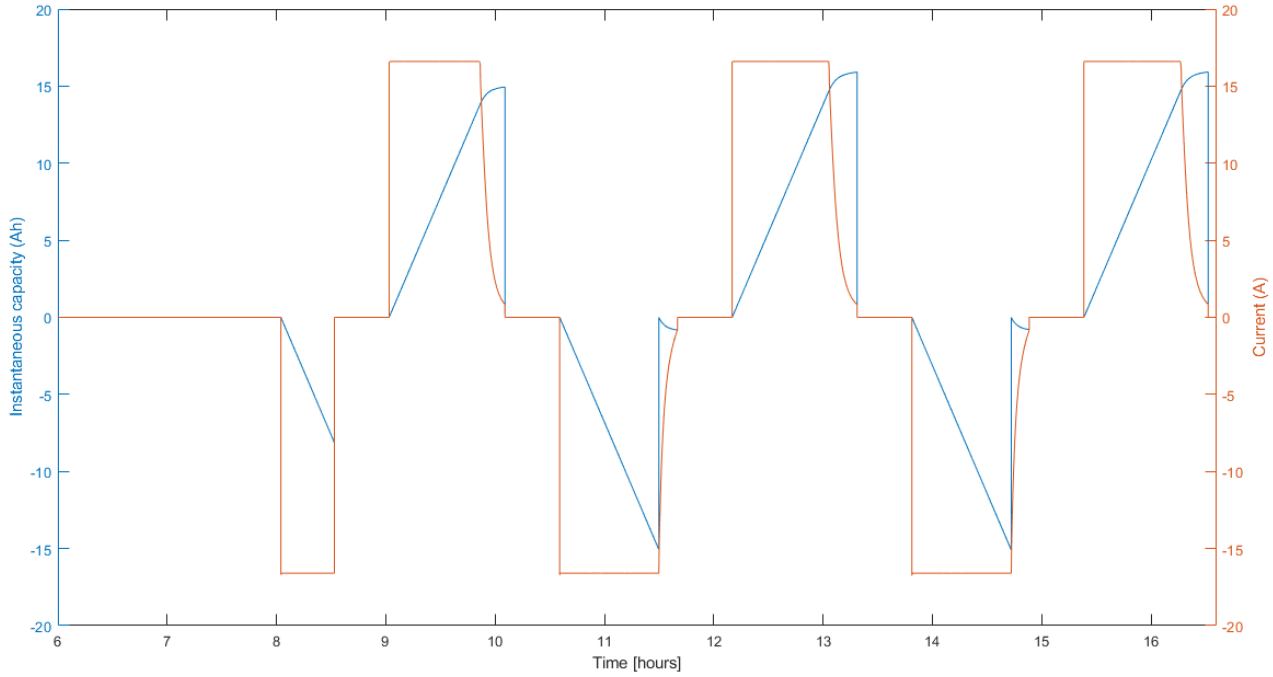

Figure 4.3. A sample plot to show the capacity evolution for the calculation of SOH

An aged cell has reduced full capacity and the number of full cycles it has gone through its life is not a linear curve with linear multiplicity. This quantity is defined by the term equivalent full cycles (EFC). The EFC can be calculated using the equation

(4.3) [50]:

$$N_{eq} = \frac{W_{tot}}{2 \times U_{nom} \times Q_{init}} \quad (4.3)$$

Here, N_{eq} = equivalent full cycles, W_{tot} = accumulated energy throughput for the cycled cell, U_{nom} = specified nominal battery voltage, Q_{init} = measured initial battery capacity

The capacity evolution or deterioration is studied with respect to changes in SOH and equivalent cull cycles (EFC). These conditions are checked for the cells of the three geometries for different conditions of temperature and cycling current rates. These results are discussed in the next chapter.

4.3.2 Temperature developed over cycling

To determine the temperature gradient over the three geometries at similar conditions, the temperatures were measured for the first extended check-up (ECU) cycle with different cycling current rates. In all the cases, the charging was done with a rate 1C, but the discharging was tested with slow to faster C-rates.

The temperature sensors used for the tests were the Negative Temperature Coefficient (NTC) sensors. This is the most commonly used type of temperature sensors, and in this case, the temperature shows an inverse relation with respect to the resistance. [51] NTC thermistors are high precision and can give a resolution and accuracy as low as 5mK.[9] The different stages of the charging and discharging were identified by using the data for the cell voltage.

The method used for the automated calculation of the SOC is the coulomb counting method. The coulomb counting method measures the discharging current of a battery and integrates the discharging current over time to estimate SOC. Coulomb counting method is done to estimate the SOC_t, which is estimated from the discharging current, $I(t)$, and previously estimated SOC values, SOC_0. SOC is calculated by the equation (4.4) [52]:

$$SOC_t = SOC_0 - \frac{\int_0^t I(t)dt}{Q_n} \tag{4.4}$$

where, Q_n is the nominal capacity measured in the beginning of cycling, and t is the time at which the SOC needs to be calculated.

[9] The temperature sensor data has the potential to be improved by using embedded temperature sensors in the case of pouch cells or temperature sensors in the jelly roll structure of the prismatic and cylindrical cells

4.3.3 30s pulse test

In this work, the internal resistance has been calculated for 30s charge and discharge pulses at the 0.5s, 10s and 30s time-instants. This section discusses the experimental procedure for the same.

Two types of pulses are used during the test: one for increasing the SOC and another 30s pulse for measuring the internal resistance. While charging, first the SOC is determined for a fully discharged cell and a pulse of 1C is applied for 30s at that SOC. Next, the cell stabilizes for a while without a pulse and then it is charged again at 1C this time to increase its SOC. In the case of discharging, the only difference is that a current is drawn from the cell. This is explained using Figure 4.4.

This method is used for the SOCs: 5%, 10%, 20%, 30%, 40%, 50%, 60%, 70%, 80, 90% and 95%. Further, for each 30s pulse, the internal resistance is calculated at the 0.5s, the 10s and 30s instant. This is done by calculating the instantaneous change of voltage in and dividing it by the current at that time in Figure 4.4 (which is approximately equal to 1C), as shown in the equation (4.5):

$$IR = \frac{\frac{\partial V}{\partial t}}{I} dt \tag{4.5}$$

Where, ∂V refers to the infinitesimal change in voltage over ∂t in Figure 4.4 and I refers to the current at the stage (which is usually constant at 1C or 16A)

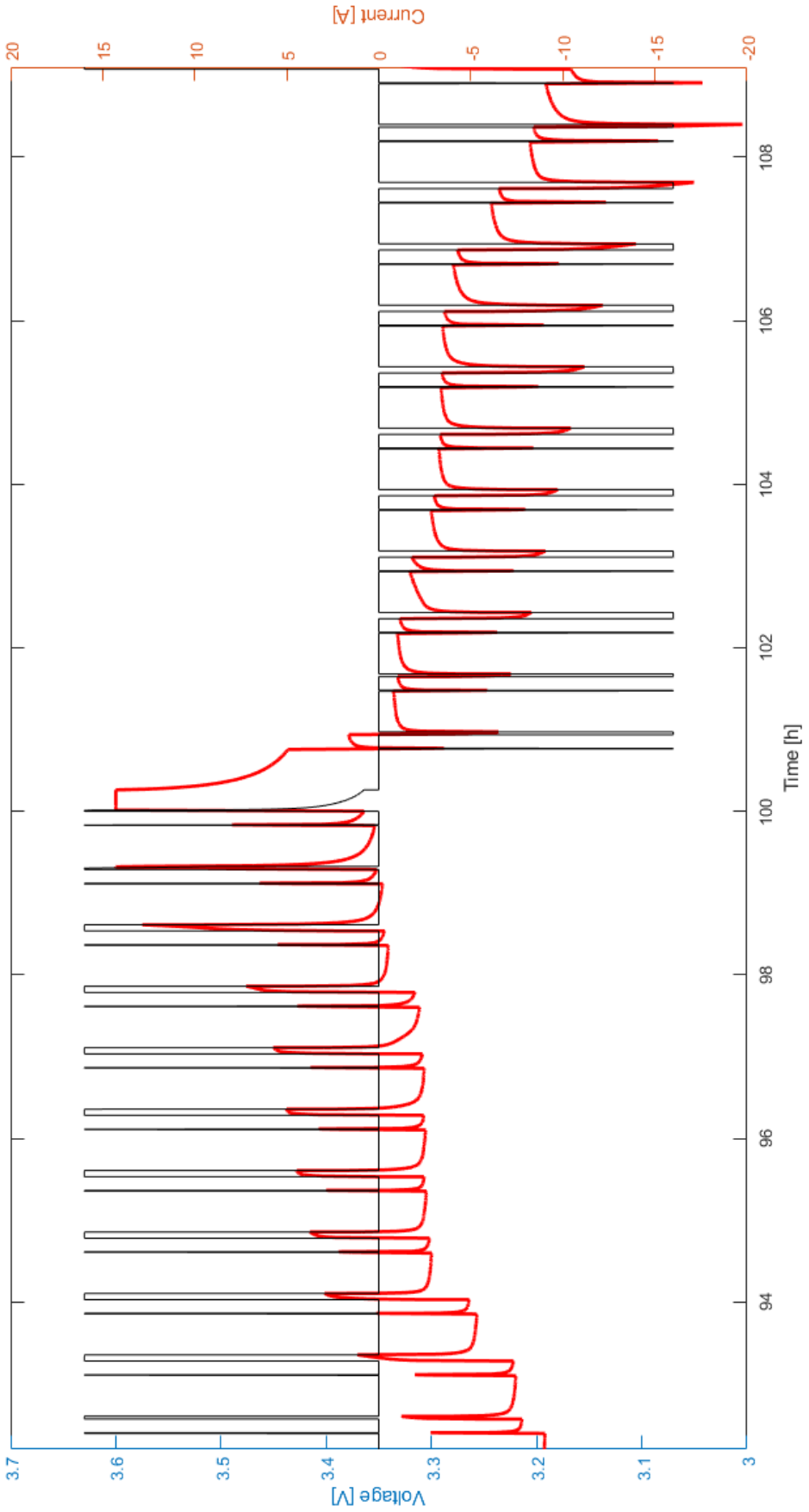

Figure 4.4. Explanation for a 30s pulse test with current pulses and voltage evolution

5 Discussion

MATLAB Data Processing and Visualization was used to extract, sort, edit and visualize the experimental data for ease of analysis. It was found that the data for cells under the same conditions of cycling rate and temperature show similar results and therefore the cell data were averaged. Further, in certain cases, data interpolation and extrapolation to maintain uniformity. The following sub-sections would discuss the experiment results from the previous chapter along with any assumptions made in each case.

5.1 Reception test data discussion

The study of the cell chemistry and materials shows the measured values for parameters like cell weights, capacity and energy densities. As discussed, a possible reason for the lower weight of the pouch cells is due to its light-weight aluminum pouch cover and lack of any hard covering. A weight analysis of the different components of the cells is also done in Figure 4.2. The difference in the weights of the prismatic (heavier) and cylindrical cells can be explained using the higher surface area of cover for the case of the prismatic cells leading to higher requirement of metallic cover material. The added weight is the case of the prismatic cells can also be attributed to an added metallic/steel support for stability. [21] In a pouch cell, the cathode, separators and anode are stacked instead of wound, as can be seen in Figure 2.3. This approach increases packaging density to the maximum and saves weight, thus increasing energy density of the cell. The packaging density when grouping cylindrical cells is low due to their round shape, and the cell case is comparatively heavy. [21]

Due to the weight comparisons as discussed, it is not surprising that energy density (Wh/kg) of pouch cells is the highest followed by cylindrical cells followed by prismatic cells. (Considering that all the cells have a capacity close to 16Ah and a nominal voltage has been assumed to be the same at 3.2V).

While all the cells have been manufactured to be around 16Ah, Table 4.1 shows a minor difference in the capacities of the cells. While cylindrical and prismatic cells are almost equal to 16Ah (cylindrical slightly higher), the capacity of pouch cell is slightly below 15Ah. A look at the Figure 4.2 can provide a possible reason for it. It shows that weight of electrode collector + electrode coating + electrolyte material is clearly less in the case of pouch cells as compared to prismatic and cylindrical geometries. The less electrode + electrolyte content in pouch cells might explain the reduced capacity.

The next sections discuss first the performance of a new unaged cell with respect to internal resistance profiles from pulse test and then the temperature evolution over cycling of each geometry. The section after that discusses the effect of aging on the cells, namely, the capacity deterioration and equivalent full cycles at different conditions of temperature and cycling, and the influence of aging on internal resistances. For ease of study and data representation, all the data values for the same geometry and same test conditions are averaged out.

5.2 Performance of unaged cells

The data obtained from the tests are then pre-processed by averaging the values for the same geometry and same test conditions (C-rate and temperature). Also, for simplicity, only the data for 0.3C-rate condition are considered.

5.2.1 Internal resistance at 100% SOH for different cell geometries

The unaged cells are subjected to the 30s pulse test as explained in the previous chapter. This internal resistance data was calculated over different SOCs of the cycling process, to represent the pulse polarization curve at every SOC considered.

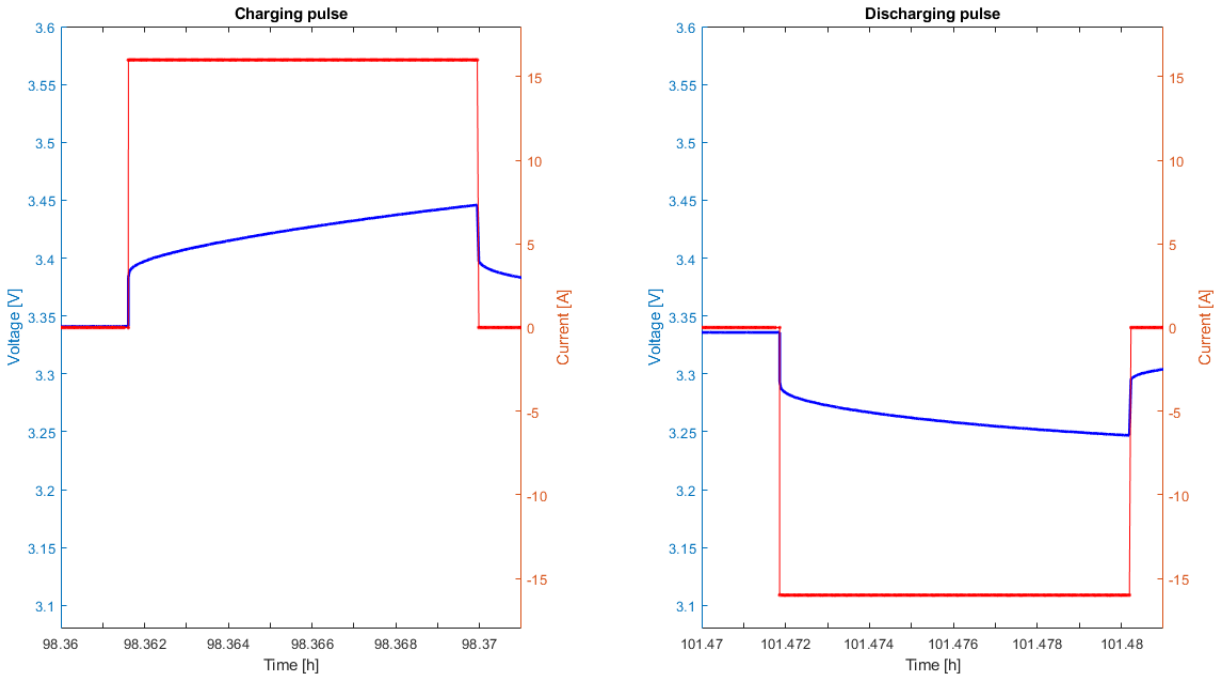

Figure 5.1. Sample current and voltages curves for 30s charge and discharge pulse

Figure 5.1 depicts sample current and potential drop curves for 30s charge and discharge pulses. The sample data is taken from a test done on a cylindrical cell for respective SOCs. Figure 5.1 resembles the schematic depicted in Figure 3.4 which shows cell voltage response to discharging pulses. Therefore, overpotentials and associated resistances can also be depicted like the schematic. In this thesis, the internal resistances for each SOC are measured for the 0.5s, 10s and the 30s instants. These time instants can be used to represent different phenomena within the cell function. The 0.5s represents the ohmic resistance; the 10s instant depicts the charge transfer reaction at the electrode-electrolyte interface and the Li^+-electrolyte concentration gradient formation (lithium mass transport phenomena) and the 30s instant shows the lithium-ion diffusion. The internal resistances at these instants represent the barrier to each phenomenon.

The first observation from the curves is the low internal resistance in pouch cells in general as compared to the other two geometries. This is expected because of the thin electrode slices used to stack together in pouch cells. Thinner the electrodes, lesser the transport path for the ions, and therefore, lesser the internal resistance. Though it is interesting to note that the internal resistance in pouch cell is higher at the extreme ends of the SOC, that is, at 0% and 100%. A slight increase in internal resistance is also observed for all geometries around the 60-70% SOC range.

The resulting data comparison between the different cell geometries is represented in Figure 5.2 and Figure 5.3. The cells represented in the figures are all conditioned at 0.3C and 5°C.

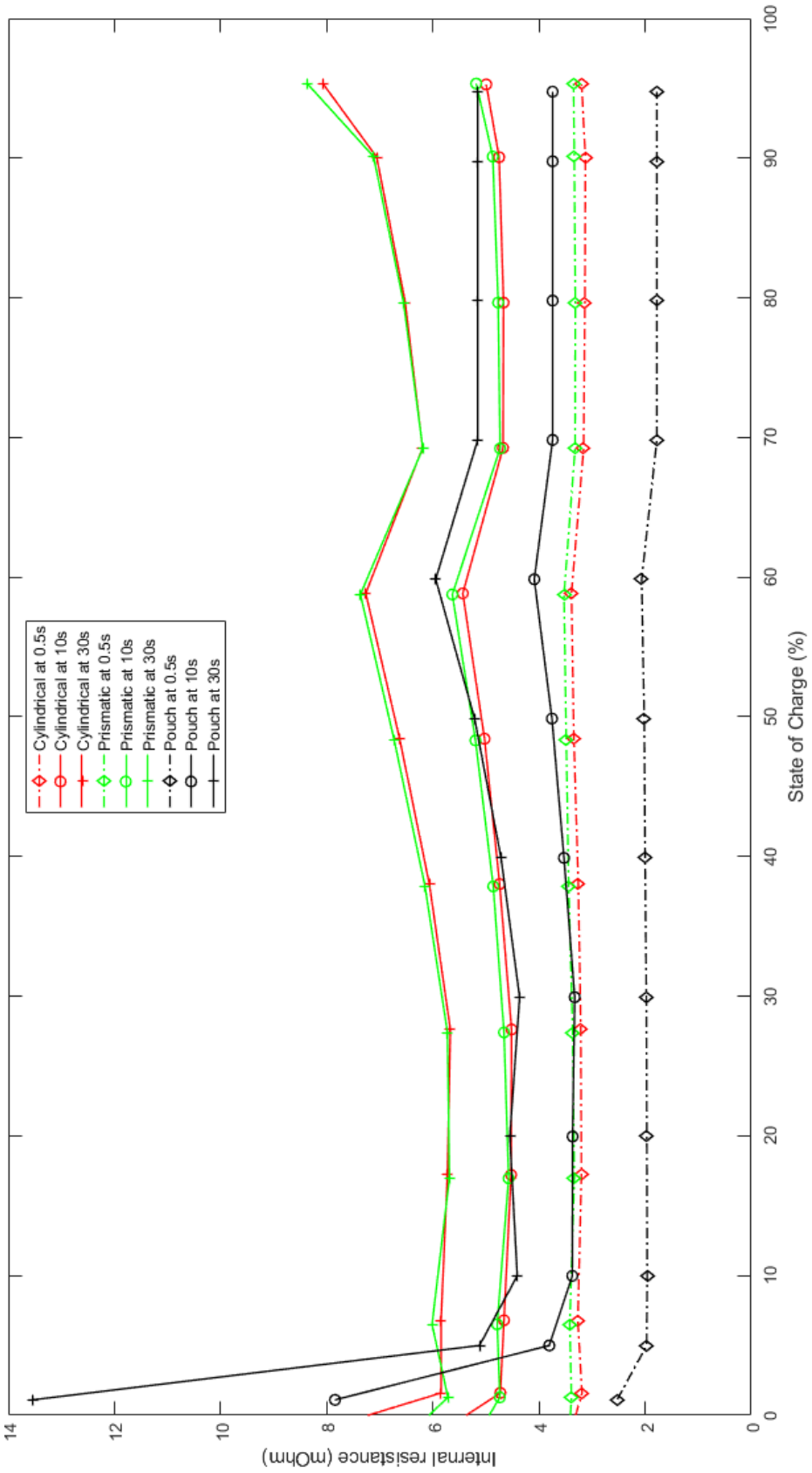

Figure 5.2. Internal resistance comparison for a charging pulse

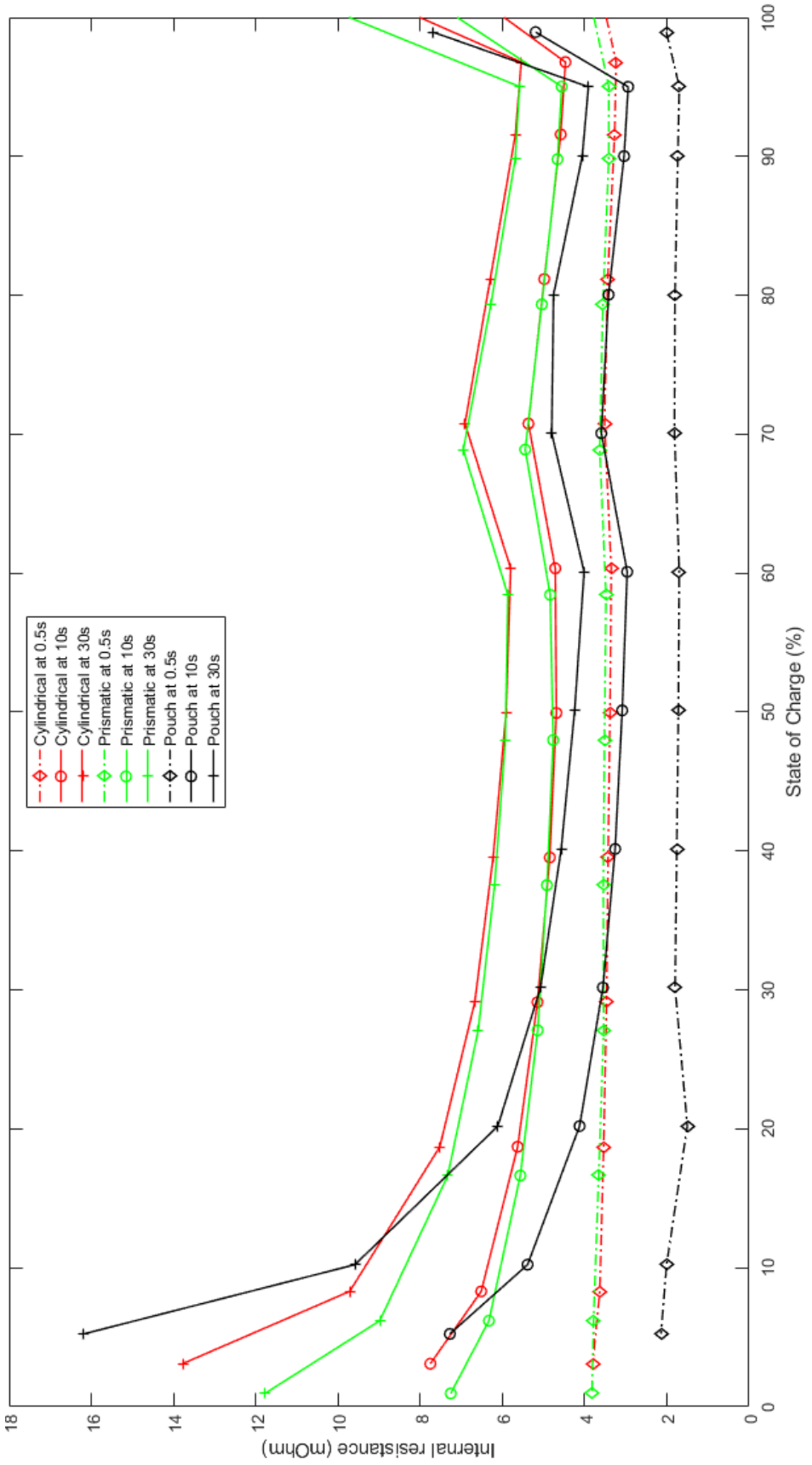

Figure 5.3. Internal resistance comparison for discharging pulse

It must be mentioned that this test was done for an unaged cell, so the initial cycling process is accompanied by the consumption of lithium-ion and electrolyte to the bulk irreversible SEI formation. For convenience, internal resistance values from the curves above are documented for SOCs of 5%, 50% and 95% in Table 5.1.

Table 5.1. Internal resistance at selected SOCs for charging and discharging pulses

	5% (in mOhm)			**50% (in mOhm)**			**95% (in mOhm)**		
Pulse instant	*0.5s*	*10s*	*30s*	*0.5s*	*10s*	*30s*	*0.5s*	*10s*	*30s*
Charging pulse for cells at 5°C/0.3C									
Cyl	3.241	4.682	5.845	3.343	5.026	6.626	3.196	4.995	8.059
Pris	3.411	4.773	5.929	3.486	5.197	6.727	3.349	5.183	8.367
Pou	1.972	3.806	5.122	2.017	3.756	5.214	1.779	3.743	5.155
Discharging pulse for cells at 5°C/0.3C									
Cyl	3.741	7.299	12.29	3.381	4.686	5.909	3.225	4.455	5.530
Pris	3.792	6.538	9.616	3.516	4.764	5.927	3.411	4.558	5.582
Pou	2.142	7.278	16.19	1.72	3.085	4.242	1.697	2.940	3.906

As discussed above, 0.5s values can be approximated to represent the ohmic resistance comprising all the electronic and bulk ionic resistances. Ideally the ohmic resistance calculated must be the instantaneous resistance calculated at the onset of the pulse, but this is limited by the measuring instrument's data acquisition capacity which is around 0.5s in these tests. [39] The ohmic resistance of pouch cells are in general the least for all conditions of SOC while it is the highest for prismatic cells. The 0.5s instant resistances or the faster dynamic effects are relatively uniform over the entire SOC range, both for the cases of charge and discharge. In general, the higher the electrode potential, the harder it is to remove a lithium from a site within the host matrix. On discharging a cell, lithium is transferred from a high energy state in the anode to a low energy configuration in the cathode, hence, the resistance values for discharging should be higher than that of charging. [39] As shown in the values in Table 5.1, the ohmic resistance is generally higher in the case of discharge

with respect to charge, except for pouch cells at the SOCs of 50% and 95%. This anomaly of pouch cells at higher SOCs may refer to an ease of extracting lithium from the anode at these states. This could indicate the formation of the SEI layer during charging at the early stages of cycling.

The 10s instant represent the slower dynamics or the charge transfer resistance which is attributed to the charge transfer reaction at the electrode/electrolyte interface. It also includes the mass transfer of Lithium-ions. The curves for all the geometries follow the tub or upward parabolic shape, with increased resistance values at the SOC extremes. The peaks are more pronounced at the start of charging or end of discharging, i.e., at low SOC values. The flattened progression of internal resistance in the middle is explained by more reversible kinetic and mass transport effects, with identical concentrations of products around the 50% SOC region. An interesting trend is seen around the 60-70% SOC range where the resistance curve shows a local peak for all the geometries. Since these local peaks are present in the case of both charge and discharge (and at the 30s instant), it could be due to the chemical state of the reactants and products at these stages of SOC and may represent a characteristic of the 16Ah $LiFePO_4$ | Graphite cells tested.

Comparing the resistance values among the geometries, the internal resistance of pouch is the least in most of the cases except for the end of the discharge cycle (low SOCs) where it surges ahead. For most of the cases, the internal resistance of the prismatic cell is the highest. Contrary to the expected trend, the resistance values at discharging are less than charging except for the low SOC stage. This is further proof that the irreversible SEI layer formation during charging is incomplete, and the extraction of lithium from anode discharge is still more favorable.

The resistance at the 30s instant represents the slowest dynamic or the rate determining step and corresponds to the lithium diffusion into the active electrode material. The resistance value at this time instant is the highest as compared to the 0.5^{th} and 10^{th} second instants. Yet again, pouch cells show the lowest internal resistance values for all cases except at the end of the discharge cycle where its resistance is significantly higher than the other two geometries. As noticed with the 10^{th} second instant, there is a local peak on the resistance curve at around 60% SOC (for charging) and 70% SOC (for discharging), could indicate a characteristic of the 16Ah $LiFePO_4$ | Graphite cells used. Another recurring trend is the higher value of the charge resistance as opposed to discharge resistance for mid to higher SOC values, which could further prove the ongoing SEI layer formation during charge.

Summarizing the results of the pulse test on an unaged cell, the pouch cell has the least resistance value among all the geometries, while the resistance of the pouch cell being

slightly higher than cylindrical cells in most of the cases. Though another characteristic trend is the elevated internal resistance value of pouch cell at the SOC extremities for the 10th and 30th second pulse instants, especially at the end of the discharge cycle where it rapidly surges ahead of the other two geometries. A characteristic local peak of internal resistance of the cells tested in this work was observed around 60% SOC region for charging and 70% SOC region for discharging. Further, there was enough evidence to prove the ongoing process of SEI layer formation during charging of the cells at the time of testing.

5.2.2 Temperature developed over cycling

One of the major safety issues in commercial Lithium-ion batteries especially in EV and HEV is associated with the temperature developed over the cycling period. Therefore, it becomes an important parameter for cell performance evaluation. Data for temperature developed is processed from the first ECU of unaged cells. For uniformity, the temperature profiles were plotted for cells stored at 0.3C and 5°C. During the cycling, the charging was done at 1C, but the discharge was done at 0.2C, 0.5C, 1C and 2C. Figure 5.4 shows the temperature evolved over the cycles for the three geometries, along with the voltage of the cells to represent the cycles.

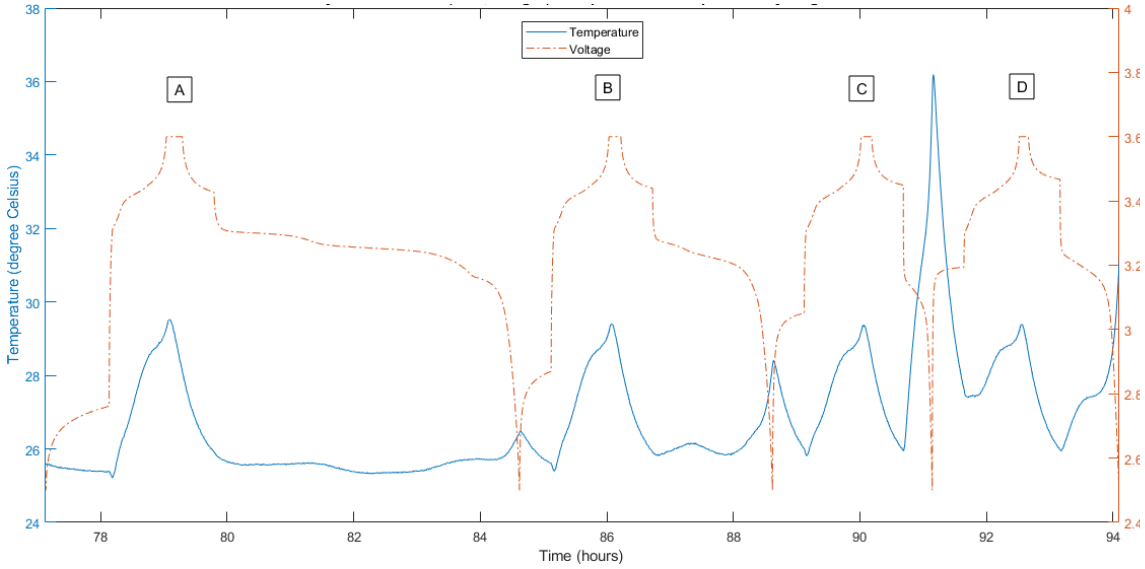

(a)

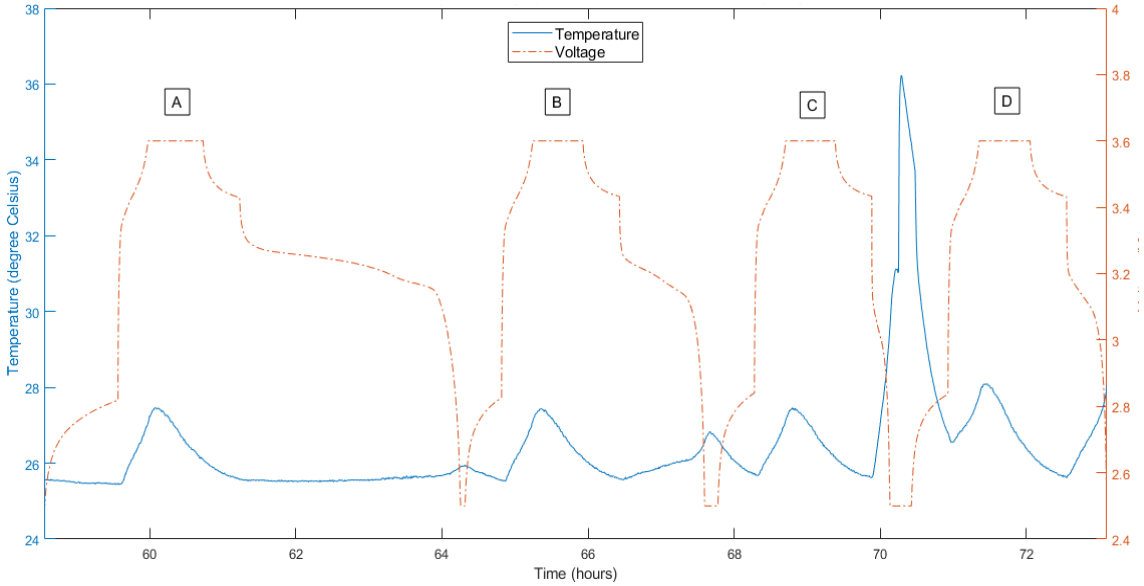

(b)

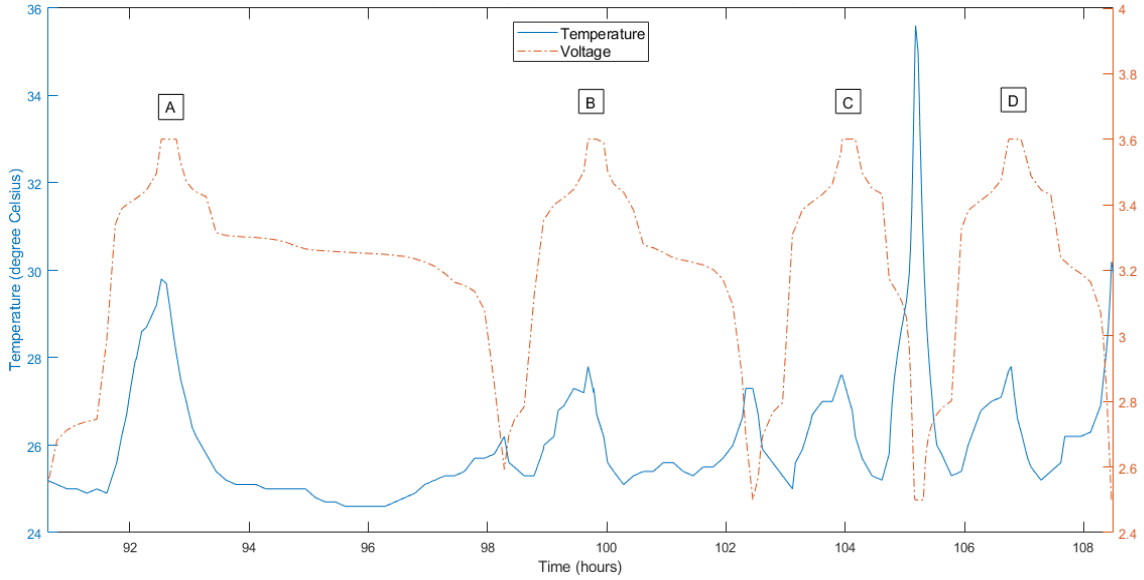

(c)

Figure 5.4. Temperature developed over cycling for (a) Cylindrical, (b) Prismatic, (c) Pouch cells

The labels in the figure refer to one cycle each and are characterised by the C-rates as shown in Table 5.2.

Table 5.2. Table showing the cycle characteristic denoted by labels in Figure 5.3

Label	**A**	**B**	**C**	**D**
Charging	1C	1C	1C	1C
Discharging	0.2C	0.5C	2C	1C

The temperature profile shows a common trend among all the geometries. There are two local peaks for each cycle, one at the end of the charging cycle and one at the end of the discharging cycle. The temperature at the end of the charging cycle (at the rate of 1C) remains almost same at the end of all the charging cycles, except for the first charging cycle of pouch cell where it is slightly higher than the subsequent cycles. Table 5.3 shows the temperature gradient developed between the beginning of the charging cycle and the peak temperatures.

Table 5.3. Temperature gradient developed at different charge/discharge cycles

Cell Type	**First 1C Charge (°C or K)**	**1C discharge (°C or K)**	**2C discharge (°C or K)**
Cylindrical	4.14	1.83	10.19
Prismatic	2	1.34	10.51
Pouch	4.8	2.5	10.30

The first column in the table shows the temperature gradient during the charging cycle at 1C (the local peak) with respect to the temperature at the beginning of the cycle, while the next two columns show the gradient at the end of 1C and 2C discharge with respect to the temperature at the start of the cycle.

A significant observation is the global peak in temperature developed at the end of the 1C charge - 2C discharge cyce for all geometries. Figure 5.5 shows a a zoomed in section

for this cycle on the same scaled axis. For each cell, the intitial temperature at the start of the whole cycle, the temperature peak at the end of the first charging cycle and temperature peak at the end of discharge cycle are also mentioned. Please note that the difference in time scale is not a significant factor as all data is for the first ECU of all geometries.

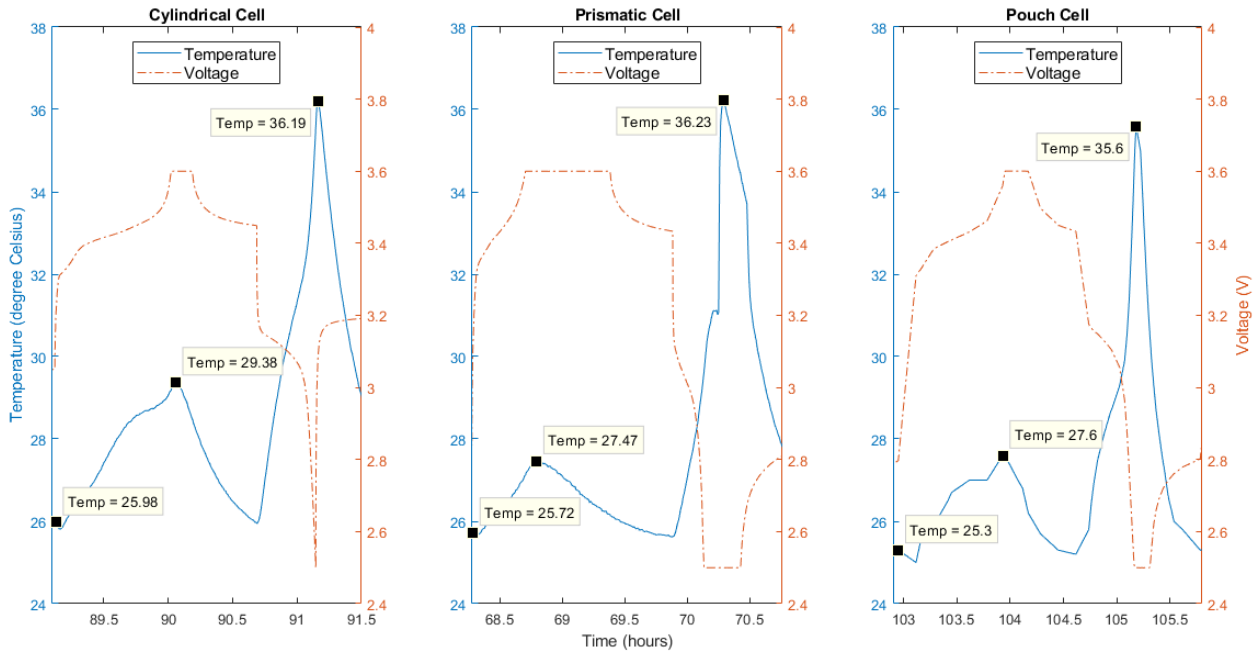

Figure 5.5. Temperature profile for 1C charge and 2C discharge for all three geometries**.**

The local peak temperature at the end of the charging for the case of the cylindrical cell is higher than the other two geometries. But, the maximum temperature developed in each case remains the most important parameter for this study.

For the 1C charge-2C discharge case, while the temperature gradients are almost similar, the absolute temperature at the end of the 2C discharge is slightly lower for the pouch cell. It is corroborated from the results of the 30s pulse test where the ohmic resistance (which leads to heating) of pouch cells is the least with prismatic cells having the highest value. This is a reasonable conclusion since the problems with thermal management and a lack of proper passage for waste heat in prismatic cells are well known. This mostly because of the higher mechanical stresses. [21] This leads to the temperatures building inside especially when subjected to rapid discharging currents. A cylindrical cell has the least surface area for heat dissipation [53], which explains the higher temperatures developed in it. As discussed earlier, pouch cells usually use thin slices of electrodes and separators which are stacked in layers. Thin electrodes can enhance the fluency of ion diffusion and improve the electrochemical reactions which helps high rate discharges and long term performances due

to the mild temperature variation [53], which might also indicate the lower temperature developed in pouch cells and no rapid increase at 2C.

Summarizing the temperature profile results, it is observed that the peak temperatures are generated at the end of charging or at the end of discharging, while higher temperatures are reached for higher C-rates. This is because over both charge and discharge, the Li ion migrate inside the cells to establish a concentration gradient, which generates heat as a function of applied current [54]. These temperatures are higher at the end of the discharge, which increases with increase in discharge C-rate from 0.2C to 2C. It is expected that the temperature rise will be even higher at higher C-rates.

Better results can be expected by testing at discharge rates higher than 2C. Further a more comprehensive study can be done with monitoring the internal temperatures developed in the cells by using embedded temperature sensors in the case of pouch cells or temperature sensors in the jelly roll structure for prismatic and cylindrical cells.

5.2.3 Summarizing unaged cell tests

In this sub-section, the tests done on the unaged cells were analyzed and discussed. These were namely: 30s pulse test for determining the internal resistance (ohmic and polarization resistances) and the temperature profile tests for different charging and discharging cycles. A correlation between the two cells were observed with the lower ohmic resistance in the case of pouch cells showing low temperature developed in them during cycling. The results were supported using literature. Further certain characteristics common to all the cell geometries were also established, for e.g., the internal resistance peaks at the 60-70% SOC marks both during charging and discharging, and the temperature highs at the end of charge or discharge. Based on these results, the three cell packaging geometries were compared for performance when unaged and relatively new.

5.3 Aging effects on cells of different geometries

The previous section discusses the performance of unaged cell. This section discusses the behavior of the cells during aging at the given temperature and C-rates. First, the capacity deterioration is discussed with respect to the equivalent full cycles (EFC). The next subsection discusses the effect of aging on the 30s pulse test results for the selected conditions of temperature and C-rates.

5.3.1 Aging characteristics over equivalent full cycle (EFC)

The concept of equivalent full cycles (EFC) has already been discussed in the previous chapter. Because of aging, the way one whole full cycle is defined differs from one time-step to other. The capacity itself undergoes changes because of the cyclic and storage deterioration. Different cell chemistries therefore show different drop in capacities and different number of equivalent cycles possible over that the aging period. Figure 5.6 shows the equivalent number of cycles for each geometry of cell for different cell conditions over the aging period as shown by the State of Health (SOH). As discussed already, the SOH has been determined by drop of capacity of the cells, therefore SOH is used as the parameter to describe the aging process.

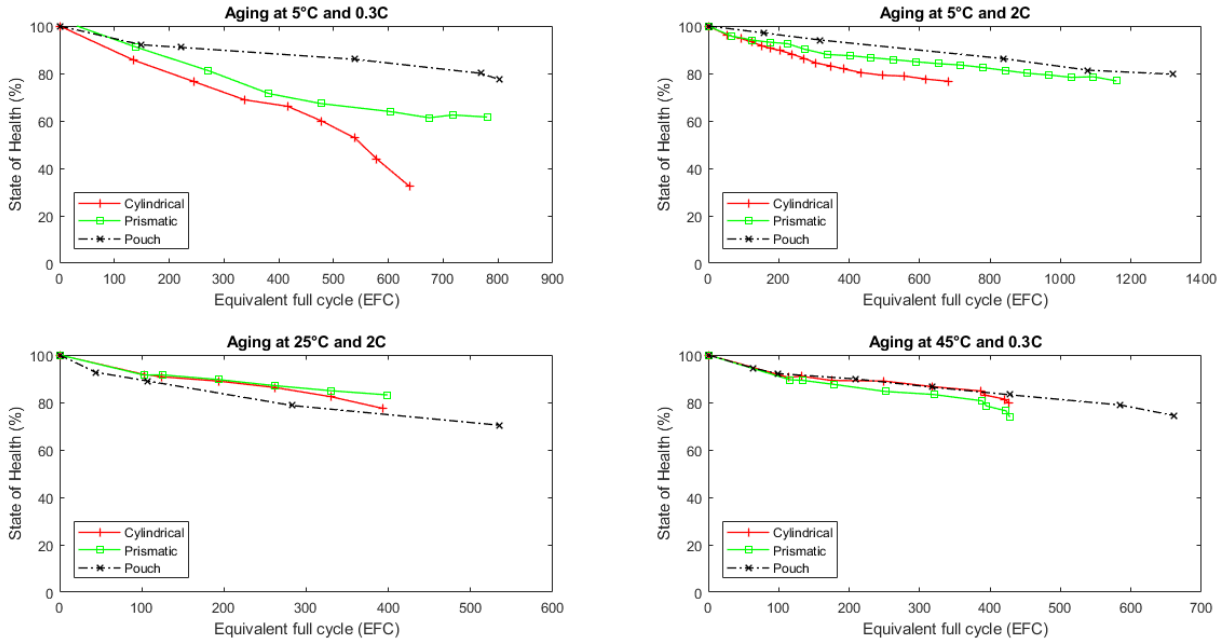

Figure 5.6. Capacity deterioration and the number of equivalent cycles obtained over the aging period for different cycling conditions.

As already discussed in the earlier chapters that the charging/discharging protocol used in these experiments, namely the constant current-constant voltage (CC+CV) and constant voltage (CV) protocols, leads to a rapid deterioration of cell capacity as compared to other charging protocols. But all the cells are expected to have had the same effect on their aging because of that. Another major influencing factor on the capacity fade is the depth of discharge (DOD), but it has not been considered here as all the cells are cycled between 0% and 100% SOC.

In electrochemical terms, the major cause of aging is because of the degradation of electrodes. [25] The aging phenomenon in Lithium-ion cells is associated with the formation of a solid electrolyte interface (SEI) layer formation on the anode. The SEI layer is formed from the lithium inventory of cathode and electrolyte salt. It is vital to the performance of the Lithium-ion cell since the entirety of the anode must have a uniform layer of SEI to prevent further disintegration of the electrolyte. Therefore, the initial cycles of Lithium-ion cell operation show a considerable drop in capacity due to the irreversible SEI layer formation out of the lithium inventory. [55] This is observed as an initial high rate of loss of capacity followed by reduced loss rate in Figure 5.6.

An optimized SEI layer is expected to have negligible electrical conductivity, high electrolyte diffusion resistance while having high lithium selectivity and permeability. Once it is properly formed, further decomposition reactions with salts and solvents are prevented as electrons cannot transfer to or through the layers. Properties of an ideal SEI formation are high electrical resistance, high lithium selectivity, high strength, tolerance to expansion and contraction stresses. [55]

In real cases, the SEI-layer thickens by repeated cycling gradually due to electron exposure to electrolyte and electrolyte diffusion to graphite surface. This not only leads to electrolyte decomposition but also might lead to loss of active lithium. [55] The four different aging mechanisms attempt to explain various ways in which this can happen. Therefore, this study primarily analyses the aging phenomenon with respect to the SEI layer formation and the related four aging mechanisms. [25] It must also be noted that most studies agree to deal with the cycle number as the main time notion, and therefore, the aging curves here are plotted against the equivalent full cycle. While in practice higher C-rates should accelerate the aging of the cells, but in practice, the relation between C-rates and the capacity fade is found to be complex. [25] [26] Even so, the highest C-rate in this study (2C) does not have significant effect on the aging mechanism. Aging and SEI layer formation strongly depend on the cycling temperature. There is an optimum temperature (usually moderate temperatures) for cycling which may be different for each cell. Temperatures above this favors further SEI layer formation and thus, accelerates aging. [56]

A first look at the aging curves in Figure 5.6 show a low capacity degradation in the case of pouch cells as compared to other geometries in all but one operating condition (25°C, 2C). For a thorough analysis, the capacity after 400 equivalent full cycles (EFC) are tabulated all the geometries under all operating conditions. It is shown in Table 5.4.

Table 5.4. Table showing the remaining capacities of cells, in terms of SOH, after 400 cycles (EFC)

Cycling conditions	**Remaining capacity in terms of SOH after 400 EFCs (%)**		
	Cylindrical	**Prismatic**	**Pouch**
5°C, 0.3C	66.69	70.70	88.13
5°C, 2C	81.40	87.49	92.84
25°C, 2C	76.94	83.12	74.82
45°C, 0.3C	82.63	78.10	84.02

In cylindrical cells, the capacity fade at 5°C and 0.3C is the lowest. But any increase in either the C-rate or the temperature leads to a slower capacity fade. This directly indicates the influence of the aging mechanism related to Lithium plating. Low temperatures affect the anode kinetics and results in the reduction of the solid state ionic diffusion rate, which increases the risk of Lithium plating. At higher C-rates or temperatures, the anode kinetics improve and thus resulting in reduced cell degradation rate, with higher temperatures being more suitable for maintaining a higher capacity. [24] Further the higher degradation rate for the case of the cell at 25°C, 2C is attributed to the combined effect of higher temperature developed due to the cycling temperature and higher cycling rate (it was observed in a previous section that temperature developed in cylindrical cells at 2C charge rate is the highest). Higher temperatures developed due to the combined factors can damage the morphology of the SEI layer leading to decomposition of the electrolyte. A further aging mechanism can be particularly seen in the case of cylindrical cell at 5°C and 0.3C, which is the loss of active material (LAM), characterized by the abrupt capacity losses during the latter stages of aging, which indicates structural degradation of electrodes at this stage. [24] Minor evidence of LAM is also seen at the end of the curve at 45°C and 0.3C.

For the case of prismatic cells, the trend resembles cylindrical cells, but with a lower rate of capacity deterioration. This might be because of Lithium plating but at a lower degree. Further, no evidence of hidden capacity loss due to LAM is seen in this case, except for a minor evidence of it at 45°C and 0.3C resembling the cylindrical cells at the same condition. This follows expectations as loss of active lithium (or LAM) is rather higher at elevated temperatures.

The pouch cells have the best capacity retention out of all the geometries under most cycling conditions (except one anomalous condition of 25°C and 2C). Since all the graphite anode based Lithium-ion cells show initial aging due to the formation of SEI layers on the electrode, it can be inferred that the SEI layer in the case of pouch cells not only has the minimum surface area but is also the most uniform and most stable. [24] [25] [55] This might be because of the less mechanical and thermal stresses in the geometry of pouch cells due to the stacked structure and soft casing. This can potentially be a significant advantage of pouch cells compared to cylindrical and prismatic geometries, with respect to SEI layer formation. This is inferred because the only factor determining the ideal SEI layer not common to all the geometries is the tolerance to expansion and contraction stresses (mechanical stresses).

The pouch cells also undergo improved capacity retention moving from 5°C, 0.3C to 5°C, 2C, resembling both cylindrical and prismatic geometries, suggesting a small Lithium plating induced LLI process because of reduced kinetics at low temperatures and low C-rate. Overall, pouch cells show a much better performance at lower temperatures. But the effect of high temperature induced SEI layer formation (temperature increase from 5°C to 45°C) overcompensates any improvement in improvement of kinetics and results in faster capacity fade at higher temperatures. It must be noted that the behavior of pouch cells at 25°C and 2C is anomalous and cannot be explained suitably with the literature studied.

Summarizing the results, it is observed that the pouch cells have the best overall capacity retention among all structures and is particularly favorable towards formation of an ideal SEI layer. Further, it is observed that all the geometries undergo Lithium plating at low temperatures of operation. A comparison of the high temperature capacity fading suggests that the optimum temperature of cycling is highest for cylindrical cells followed by prismatic cells with pouch cells having the least. Both the prismatic and cylindrical geometries show tendencies of loss of active material (LAM) with an abrupt increased capacity fade, with cylindrical cell at 5°C and 0.3C showing a significant drop. Any instances of LAM suggest a possible electrode deterioration.

After the capacity deterioration studies, the cells from two different conditions of cycling (namely, 0.3C, 5°C and 0.3C, 45°C) were chosen for 30s pulse tests to determine the effect of capacity fade on the internal resistance and the polarization in the cells.

5.3.2 Change in internal resistance by aging

The 30s pulse test, as discussed in section 5.1.1. earlier, was used on the aged cells at the cycling conditions 0.3C, 5°C and 0.3C, 45°C. The main objective was to assess the

electrochemical phenomena of the cells during capacity fade. To achieve the same, the test data were taken from the extended check-ups (ECUs). It must be mentioned that the different geometries tested were at different State of Health (SOH) at the ECUs, as shown in Table 5.5. The table also shows the number of equivalent full cycles (EFC) at that SOH (data taken from Figure 5.6). It is seen from the table that cylindrical and pouch cells at 0.3C, 5°C and pouch cell at 0.3C, 45°C are past the end of life (EOL) of a cell (when SOH<80%).

Table 5.5. State of Health (%) and EFC of cells for 30s pulse test

Geometry	**SOH (%)**	**Equivalent full cycles**
At 0.3C, 5°C		
Cylindrical	76.6	245
Prismatic	81.2	271
Pouch	75.4	840[10]
At 0.3C, 45°C		
Cylindrical	89.2	249
Prismatic	87.6	178
Pouch	74.5	661

The main objective is to analyze the general trends in the electrochemical behavior of the aged cells of different geometries over the whole SOC range. To best understand the data, the change in internal resistance values or internal resistance ratio (IRR) from the unaged cell values are plotted against the SOC for all the cells, therefore, all the y-axis values are ratio of internal resistance of aged cell to that of the unaged cells.

[10] Approximate value calculated by extrapolation

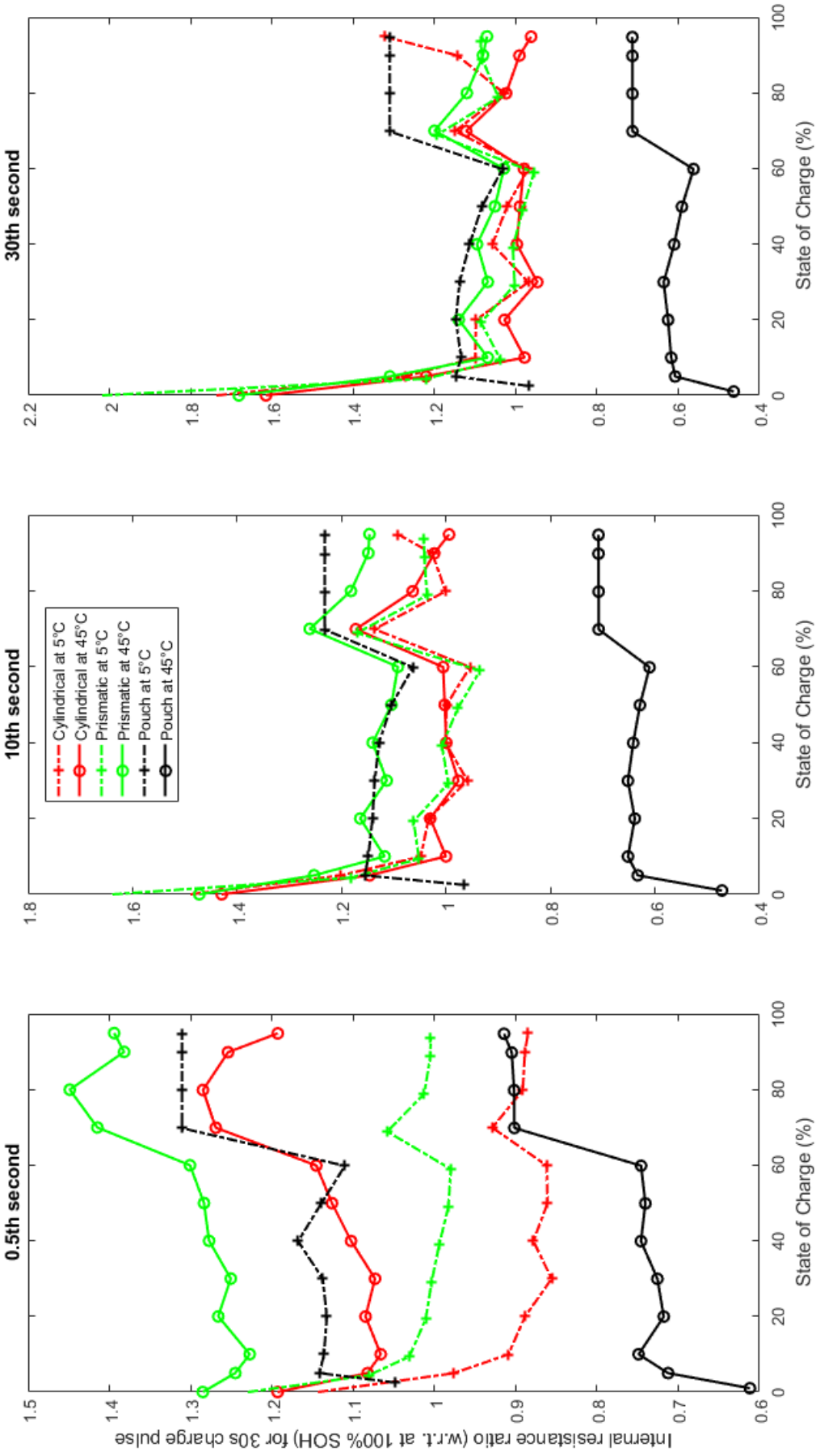

Figure 5.7. Internal resistance ratio (w.r.t. unaged cells) during 30s charge pulse test

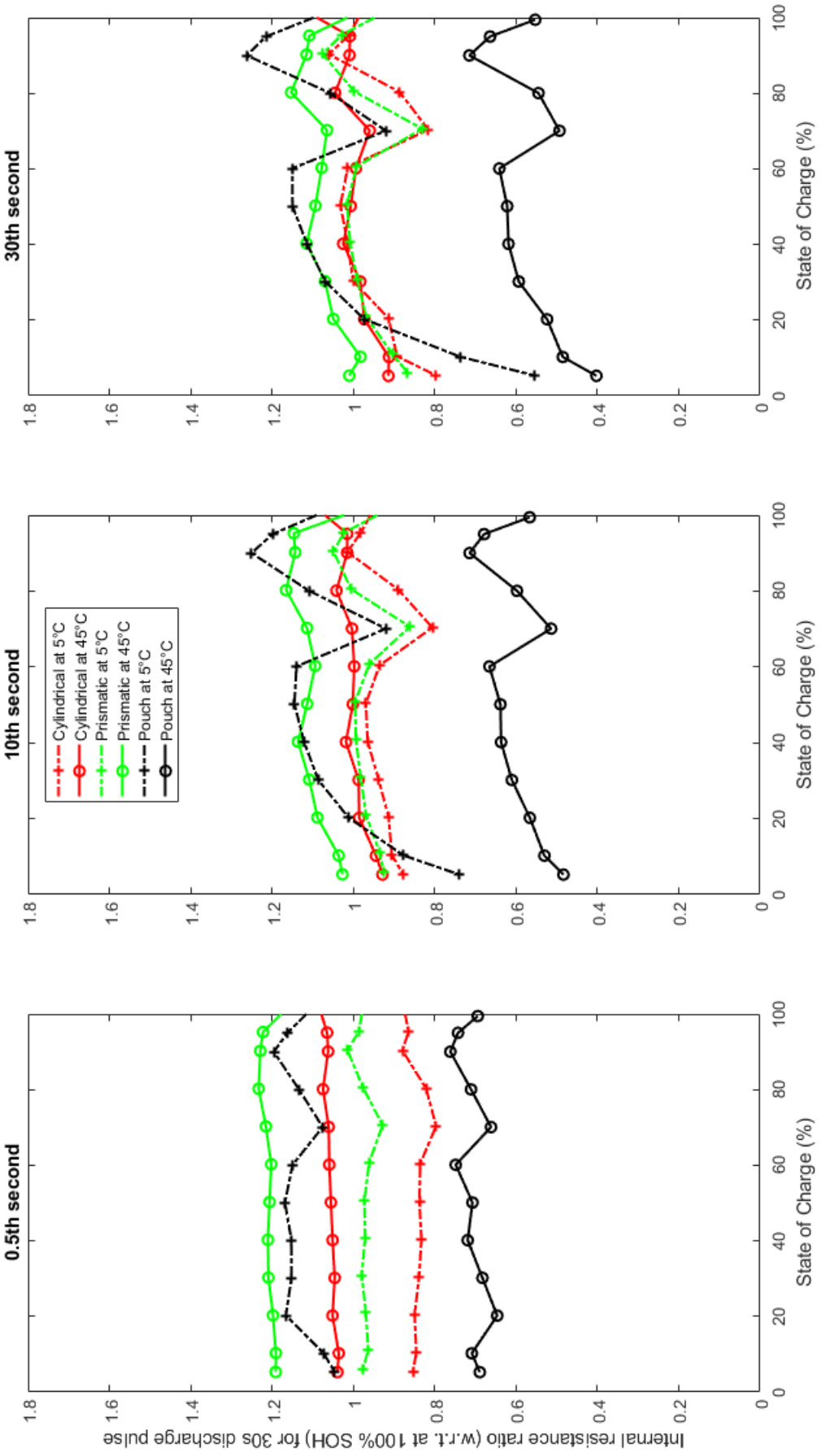

Figure 5.8. Internal resistance ratio (w.r.t. unaged cells) during 30s discharge pulse test

Since all the cells are at different SOH stages, a direct comparison between the IRR values is unreasonable. But a general comparison between the curve shapes and trends can be made. During the charging pulse, it is noted that for low values of SOC, there is an increase in the IRR for pouch whereas for the other two geometries it falls from a higher value of the ratio. Another interesting observation is that the curve for the high temperature pouch cells and low temperature pouch cells are almost mirror images but the same cannot be said about the other two geometries. For a further detailed comparison, the IRR values (obtained from Figure 5.7 and Figure 5.8) and the actual internal resistance values of the aged cells are tabulated in Table 5.6 and Table 5.7

Table 5.6. Changing in internal resistance due to aging (for charging pulses)

	5%			**50%**			**95%**		
Pulse	***0.5s***	***10s***	***30s***	***0.5s***	***10s***	***30s***	***0.5s***	***10s***	***30s***
Charging pulse for cells at 5°C/0.3C									
Cyl	3.110	5.685	7.433	2.874	5.020	6.767	2.824	5.449	10.65
76.6%	*0.976*	***1.146***	***1.273***	*0.861*	***1.002***	***1.021***	*0.885*	*0.994*	***1.325***
Pri	3.630	5.580	6.980	3.426	5.08	6.610	3.370	5.450	9.110
81.2%	***1.081***	***1.252***	***1.196***	*0.983*	***1.104***	*0.979*	***1.005***	***1.146***	***1.087***
Po	2.244	4.393	5.867	2.296	4.149	5.649	2.325	4.608	6.750
75.4%	***1.141***	*0.633*	***1.147***	***1.139***	*0.629*	***1.083***	***1.311***	*0.708*	***1.310***
Charging pulse for cells at 45°C/0.3C									
Cy	2.877	4.666	6.125	2.820	4.325	5.804	2.657	4.193	6.544
89.2%	***1.082***	***1.202***	***1.221***	***1.126***	*0.999*	*0.990*	***1.193***	***1.091***	*0.962*
Pri	3.742	5.442	6.847	3.670	5.036	6.352	3.574	5.078	7.331
87.6%	***1.245***	***1.172***	***1.310***	***1.284***	*0.977*	***1.051***	***1.394***	***1.042***	***1.071***
Po	1.497	2.497	3.333	1.627	2.476	3.190	1.708	2.768	3.809
74.5%	*0.712*	***1.155***	*0.607*	*0.740*	***1.105***	*0.591*	*0.914*	***1.232***	*0.713*

Table 5.7. Changing in internal resistance due to aging (for discharging pulses)

	5%			**50%**			**95%**		
Pulse	***0.5s***	***10s***	***30s***	***0.5s***	***10s***	***30s***	***0.5s***	***10s***	***30s***
Discharging pulse for cells at 5°C/0.3C									
Cyl	3.247	6.767	10.74	2.830	4.541	6.096	2.792	4.385	5.598
76.6%	*0.853*	*0.877*	*0.798*	*0.837*	*0.965*	***1.031***	*0.864*	*0.982*	***1.010***
Pri	3.731	6.722	10.21	3.420	4.744	6.019	3.364	4.664	5.746
81.2%	*0.976*	*0.926*	*0.866*	*0.972*	*0.994*	***1.015***	*0.986*	***1.023***	***1.029***
Po	2.150	4.720	7.070	2.010	3.532	4.878	1.972	3.524	4.745
75.4%	***1.045***	*0.740*	*0.553*	***1.168***	***1.120***	***1.149***	***1.161***	***1.198***	***1.214***
Discharging pulse for cells at 45°C/0.3C									
Cyl	3.029	5.641	8.909	2.748	3.991	5.221	2.701	3.858	4.901
89.2%	***1.039***	*0.928*	*0.913*	***1.055***	***1.018***	***1.006***	***1.064***	***1.015***	***1.008***
Pri	3.890	6.387	9.567	3.630	4.802	5.927	3.564	4.649	5.591
87.6%	***1.190***	***1.026***	***1.009***	***1.206***	***1.136***	***1.093***	***1.222***	***1.146***	***1.108***
Po	1.392	2.648	4.112	1.307	2.030	2.700	1.325	2.040	2.643
74.5%	*0.689*	*0.483*	*0.402*	*0.707*	*0.636*	*0.621*	*0.742*	*0.678*	*0.663*

In Table 5.6 and Table 5.7, the incremental values are mentioned in italicized numbers with the values more than 1 shown in bold.

It is observed from the IRRs that the internal resistances both increase and decrease for the aged cells with respect to the unaged cells. In general, the internal resistance is expected to increase with capacity deterioration. But this effect does not kick in until the latter stages of capacity drop, which is in accordance with the studies done by Lewerenz et al. [57] and Friesen et al. [58]. According to studies done by Lewerenz et al., the internal resistance is

either constant or decreasing during the cycling, and it increases rapidly only when the capacity becomes very low or cut-off voltages are reached during cycling. The start of the rapid increase in internal resistance depends on whether the aging conditions are severe (internal resistance increase at around 80-85%) or mild (internal resistance increase at around 70%). [57] Rapid capacity fade due to the aging phenomena also lead to an early onset of rapid internal resistance increase. Friesen et al. have plotted internal resistance evolution curves over equivalent full cycles (EFC) and the curves have the upward parabolic shape. The internal resistances of the cells studied by them decrease until about the first 100-150 EFCs, after which they rise and only reach values equal to an unaged cell after around 300-320 EFCs for low temperature cells and about 800 EFCs for high temperature cells. This initial decrease in internal resistance is attributed to the formation of a more effective SEI with a lower Lithium-ion migration and charge transfer resistances. [58] These studies explain the internal resistance ratios less than 1 shown in Figure 5.7 and Figure 5.8. It must be noted, as discussed in previous sections, the 0.5s pulse instant represents the ohmic resistance, the 10s instant represents the charge transfer kinetics and mass transport, and the 30s instant represents the Lithium-ion diffusion into the active electrode material. Table 5.8 further simplifies the data and tabulates the maxima and minima of IRR and the associated electrochemical phenomena.

For the case of cylindrical cell at low temperature conditions (0.3C, 5°C), the values of IRR are between the range of a 14% decrease (ohmic resistance at 50% SOC) to a 32% increase (diffusion polarization at 95% SOC) during a charging pulse. For a discharging pulse, this range is between 21% reduction (diffusion polarization at 5% SOC) and 3% increase (diffusion polarization at 50% SOC). At this SOH of the cell (76.6%), it is seen that the polarization due lithium-ion diffusion has undergone the maximum resistance increase, while an increase can also be seen in the charge transfer kinetic component. This supports the argument in the previous sub-section that for cylindrical cells, low temperatures affect the anode kinetics and results in the reduction of the solid state ionic diffusion rate. It is interesting to note the elevated increment of the resistance during charging for the extreme ends of SOC (5% and 95%). The cylindrical cell at high temperature (0.3C, 45°C) shows a much gentler fluctuation with the charging pulse resistances being between a range of a 4% decrease (diffusion polarization at 95% SOC) to a 22% increase (diffusion polarization at 5% SOC), whereas for discharging the range is 9% decrease (diffusion polarization at 5% SOC) to 6% increase (ohmic resistance at 95% SOC). Even though the SOH of this cell is much higher than the cylindrical cell at low temperature, they have gone almost the same number of EFCs (as shown in Table 5.5). This shows a better performance of the high temperature cylindrical cells, as deduced during the capacity deterioration studies.

Table 5.8. Table showing the internal resistance fluctuation range for different geometries

	Charging pulse range	**Discharging pulse range**
at 0.3C, 5°C		
Cyl	14% decrease (ohmic resistance at 50% SOC) to a 32% increase (diffusion polarization at 95% SOC)	21% reduction (diffusion polarization at 5% SOC) and 3% increase (diffusion polarization at 50% SOC)
Pris	21% decrease (ohmic resistance at 50% SOC) to a 25% increase (charge transfer kinetic at 5% SOC)	14% decrease (diffusion polarization at 5% SOC) to a 3% increase (diffusion polarization at 95% SOC)
Pou	37% decrease (charge transfer kinetic at 5% SOC) to a 31% increase (ohmic resistance and diffusion polarization at 95% SOC)	45% reduction (diffusion polarization at 5% SOC) to a 21% increase (diffusion polarization at 95% SOC)
at 0.3C, *45*°C		
Cyl	4% decrease (diffusion polarization at 95% SOC) to a 22% increase (diffusion polarization at 5% SOC)	9% decrease (diffusion polarization at 5% SOC) to 6% increase (ohmic resistance at 95% SOC)
Pris	2% decrease (charge transfer kinetic at 50% SOC) to 40% increase (ohmic resistance at 95% SOC)	1% increase (diffusion polarization at 50% SOC) to 22% increase (ohmic resistance at 95% SOC)
Pou	41% decrease (diffusion polarization at 50% SOC) to a 23% increase (charge transfer kinetic at 95% SOC)	60% reduction (diffusion polarization at 5% SOC) to a 26% reduction (ohmic resistance at 95% SOC)

The resistances calculated during the charging for prismatic cells at low temperature (0.3C, 5°C) is more turbulent in deviating from the initial values with a range of 21% decrease (ohmic resistance at 50% SOC) to a 25% increase (charge transfer kinetic at 5% SOC). During discharging, it shows a 14% decrease (diffusion polarization at 5% SOC) to a 3% increase (diffusion polarization at 95% SOC). The increase is maximum in the case of the charge transfer kinetic, followed by the Lithium-ion diffusion. This does not fully prove the aging mechanism in the cell but shows an interesting trend with respect to cylindrical cell where the diffusion related polarization showed a higher increase. For the case of the prismatic cell at higher temperatures (0.3C, 45°C), the ohmic resistance shows an especially

highest elevation among all cells with a 40% increase during charging and 22% increase during discharging. Both these values are at 95% SOC. This is shown in red in Table 5.6 and Table 5.7. Overall, the internal resistance ratio is uniformly higher than 1 for all pulse instants at all SOCs for the high temperature prismatic cell both for charging and discharging

The pouch cells show a large fluctuation in internal resistance from that for an unaged cell. They also show very contrasting trends for cells at high and low temperatures. For the low temperature cells, the IRR is in the range of 37% decrease (charge transfer kinetic at 5% SOC) to a 31% increase (ohmic resistance and diffusion polarization at 95% SOC) for charging. The internal resistance has significantly reduced for the 10s pulse instant pointing to improved charge transfer kinetic and mass transport. But the ohmic resistance and the diffusion polarization (especially at high SOC) show a high increase. For the case of discharging of low temperature pouch cells, the IRR is in the range of a 45% reduction (diffusion polarization at 5% SOC) to a 21% increase (diffusion polarization at 95% SOC). The increase is more at higher SOCs, but overall increase is less than the case of the charging pulse. The pouch cells at high temperatures also show a high fluctuation in internal resistance values. For the case of charging, the range is 41% decrease (diffusion polarization at 50% SOC) to a 23% increase (charge transfer kinetic at 95% SOC). For the discharging pulses, range is a 60% reduction (diffusion polarization at 5% SOC) to a 26% reduction (ohmic resistance at 95% SOC). What is notable about the pouch cells is the very high number of completed equivalent full cycles (EFC) even when the IRR is significantly less than one. This indicates that the cell capacity deterioration has set in later than the other two geometries.

The lithium-ion diffusion into the active electrode material being the rate determining step, any significant increase in the diffusion polarization results in a slow reaction kinetic for the cell. For the low temperature cells, a steep increase in diffusion polarization can be seen in the case of pouch cell at low temperatures for both charging and discharging. It is also seen in cylindrical and prismatic cells, but only for the charging pulses. For the high temperature cells, the diffusion polarization increases significantly only in the case of the cylindrical cell for charging pulse. Further a low value of resistance for the 10s instant (or charge transfer kinetic) indicates a stable SEI layer formation.

The biggest electrochemical influence at any stage can be indicated by the highest resistance increase at each SOC. This is summarized in Table 5.9.

Table 5.9. Summary of the dominant resistance increase factor at different SOC values

	5%		**50%**		**95%**	
	Charge	**Dis-charge**	**Charge**	**Dis-charge**	**Charge**	**Dis-charge**
For 0.3C, 5°C						
Cyl	-	Ohmic	Diffusion	Diffusion	Diffusion	Diffusion
Pris	Charge transfer	-	Charge transfer	Diffusion	Charge transfer	Diffusion
Pou	Diffusion	Ohmic	Charge transfer	Ohmic	Ohmic	Diffusion
For 0.3C, 45°C						
Cyl	Diffusion	Ohmic	Ohmic	Ohmic	Ohmic	Ohmic
Pris	Diffusion	Ohmic	Ohmic	Ohmic	Ohmic	Ohmic
Pou	Charge transfer	-	Charge transfer	-	Charge transfer	

Summarizing the above results, it was first proved that the cell resistance does not increase for a rapidly for a first few cycles and may even decrease. The resistance rapidly increases only around the end of life of the cell or after the cut-off voltage has been reached. Further, the general trends of the curves of the incremental change of resistance over SOC was compared for the different cell geometries. While other cell geometries show decreasing IRR from small values of SOC during charging, pouch cells showed the opposite trend. Further the curves for high and low temperatures for pouch cells were found to be parallel. In the next part of the discussion, IRR values were tabulated for 5%, 50% and 95% SOCs and the corresponding trends discussed for each cell. For cylindrical cells, the values perfectly synchronize with the increase in diffusion polarization as seen for the cells at low temperatures. For prismatic cells, the ohmic resistances for 95% SOC for the discharging pulses are found to be the highest among all respective resistances for high and low temperature. Pouch cells show the maximum fluctuations in IRR with some significantly low values in some cases (especially discharging at high temperatures). Though no evidence could be found for the

aging mechanism in pouch cells, the high number of EFCs and low internal resistances indicated a reliable performance of the cell over many cycles.

5.3.3 Summary of tests on aged cells

In this sub-section, first the capacity deterioration of aged cells was studied for different conditions of operating temperatures and C-rates. The different capacity fade mechanisms were analyzed. Cylindrical cells, especially, and to some extent prismatic cells showed evidence of lithium plating at low temperatures. The performance of pouch cells was better at low temperatures. Cylindrical cells show the highest operating temperatures while the pouch cells have the least. Overall, the capacity retention of pouch cells is the best among all geometries.

Further, 30s pulse tests were performed on cells with the same C-rate (0.3C) and two different temperatures (5°C and 45°C). A direct comparison between the cells as all of them were at different SOHs during the check-ups (ECU). The tests gave information about the electrochemical phenomena. Many resistance and polarization values seemed to reduce with respect to unaged cell. This was validated using previous studies and it was inferred that the actual resistance increase kicks off around the end of life of the cells or on reaching the cut-off voltage and depends on the severity of cycling conditions. It was seen that the elevated increase in diffusion polarization concurs with the lithium plating occurring for cylindrical cells for low temperatures. Prismatic cells show an elevated ohmic resistance increase at higher SOCs while discharging. The aged pouch cells show the highest fluctuations in resistance and polarization values with respect to the unaged cells. It is also evident that the capacity deterioration and rapid internal resistance increase for pouch cells kicks in at a much lower SOH and can undergo higher number of equivalent full cycles (EFC)

6 Summary

The objective of the thesis was to analyze the performance of 16Ah $LiFePO_4$ | Graphite cells with respect to their packaging geometries. The literature studied showed limited studies on performance comparisons of lithium-ion cells of similar capacities and chemical composition. The initial chapters discussed the fundamentals of lithium-ion cells with focus on the $LiFePO_4$ cells. The different packaging geometries were introduced and studied based on their structures, illustrations and examples.

The literature reviewed discussed the state-of-the-art in the study of comparison of lithium-ion cell packaging geometries. The aging mechanisms were studied with focus on the importance of SEI layer formation and its contribution in capacity deterioration. The aging of the cell has shown changes in the internal resistance which directly affects properties like capacity, power density, energy density etc. The different types of internal resistances and the polarization resistances were discussed. Different methods to measure and separate resistance based on electrochemical stages were studied focusing more on DC pulsed methods to measure resistances. It was found that the DC pulsed method is not completely capable of separating the resistances according to the electrochemical phenomena, but a suitable approximation was used in the further tests and analyses.

The cylindrical and prismatic cells were prepared with standardized equipment available following the jelly roll manufacturing. The manufacture of the pouch cells required slow diligent and manual work, with cutting thin layers of electrodes and separator and arranging, followed by further addition of electrolyte, tab design and sealing after degasifying. Within the scope of the thesis, only cyclic aging tests were included. The cell cycling was done using the standard CC-CV method. The BaSyTec Extended Cell Test System (XCTS) was used for the cycling tests. The temperature measurement was done using standard Negative Temperature Coefficient (NTC) thermistors. The major tests performed within the scope of the thesis were the temperature evolution tests and the internal resistance measurement using the DC pulse tests.

Reception tests showed lowest weight and higher energy density of the pouch cells primarily due to the light aluminum pouch cover. Further, the zig-zag layering of thin slices of electrodes and separators is shown to have the highest packing density thus reducing the

packing material required. The prismatic cell was found to have the highest weight because more surface area required for the metallic cover compared to cylindrical cells.

The unaged cells (100% SOH) were first tested for a performance analysis. The pouch cells showed the lowest internal resistance which was attributed to the thinner electrodes and less distance for ion diffusion. It must be noted that the lithium-ion diffusion in the active electrode material is the rate determining step. The ohmic resistances are found to be highest for the prismatic cells in general. The ohmic resistance remains almost uniform for all packaging geometries for both charging and discharging. The charge kinetic polarization resistance shows a tub like progression in moving from a lower SOC to higher values. The stable mid-SOC region is associated with more reversible kinetics and mass transport due to equivalence of products and reactants around 50% SOC. For the charge kinetic and diffusion polarizations, pouch cells again show the least resistance values, except when its value shoots up at lower SOCs during discharge. A characteristic of all the cells for the charge kinetic and diffusion polarization resistances is a local peak around the 60-70% SOC region for both charging and discharging. The temperature evolution in the cells followed from the ohmic resistance of the cells with pouch cells getting the least warm and prismatic cells getting the hottest. The peaks in temperatures itself were at the end of the charge and discharge cycles, with higher current rate during discharge leading to higher temperatures.

In the next stages included the study of the behavior of aging on the capacity deterioration. First the capacity drops were plotted over the equivalent full cycles (EFC) to attempt to determine the aging mechanisms in each cell. Cylindrical and prismatic cells showed evidence of lithium plating at lower temperatures. They also showed the characteristic sudden decrease in capacity at higher EFCs which is associated with the loss of active material (LAM) due to electrode deterioration. The pouch cells have the best capacity retention over many cycles. One of the reasons for it is attributed to the uniform and stable SEI layer formed due to the less mechanical and thermal stresses in the geometry of pouch cells due to the stacked structure and soft casing. A comparison of the cycling temperatures of the cells shows that the cylindrical cells have the highest optimum temperature with pouch cell having the least. The aged cells were also analyzed with the DC pulsed test to check the effect aging on electrochemical activity. It was proved that initially the internal resistance remains almost constant or even goes down before the severity of the cycling determines when the actual rapid rise of internal resistance starts (typically around the end of life mark). The pouch cells showed evidence of a very late onset of a rapid internal resistance increase, though it also showed a large variation of resistance values over the different SOCs compared to the values of the unaged cell. Overall, the behavior of aged pouch cells to DC pulse test was quite different from the other two geometries.

7 Prospect

The rising significance of sustainability in mobility and renewable energy storage systems has necessitated the further research into cheaper and safer Lithium-ion batteries. $LiFePO_4$ | Graphite cells have become popular as safer options. But further research is required to make the technology cheaper and its application more widespread. The study of different packaging geometries opens a totally new area of research to explore the technology further. For instance, it could open more possibilities where certain applications are more suited to certain geometries. As studied in this thesis, the comparison study of cells of similar chemistry and design capacity but with different geometries is still at a very pristine stage. This thesis is a first such study of the performance analysis of these packaging geometries, which elevates the scope of this work.

The scope of this thesis can be further increased by improving on the tests performed. For instance, to get a better approximation of the temperature developed within the cell, embedded temperature sensors in the case of pouch cells or temperature sensors in the jelly roll structure of the prismatic and cylindrical cells can be used as used in some past studies. Further, the temperatures can be calculated for charging pulses at more than 1C current rate as done in this study. Temperature rise at higher C-rates, especially above 5C have shown much higher temperature rise and gives much better values for a thorough comparison. Similarly, more conditions of cycling temperature and C-rates would help in more thorough knowledge about their effects in the different geometries. The DC pulsed tests on the aged cells were done on cells of different SOHs which does not make it possible to perform a direct comparison between the geometries. Ideally, the extended check-ups (ECU) can be performed on set values of mid-of-life (MOL) and end-of-life (EOL). A post mortem studies of these cells can also be interesting. Moreover, the DC pulsed test fails to exactly separately the resistances and polarizations, and other methods like AC tests or EIS can be performed. Further, calendar aging tests can give some interesting insights into the behavior of the packaging geometries.

The purpose of this study is to pave way for further studies in this field of research. In the future, these tests can be adapted to more specific applications, for e.g., using data from testing stage electric vehicles.

Bibliography

[1] Buchmann, Isidor. 2018. BU-1003: Electric Vehicle (EV). Battery University, Cadex Electronics Inc (2018). https://batteryuniversity.com/index.php/learn/article/electric_vehicle_ev.

[2] Grandjean, Thomas; Barai, Anup; Hosseinzadeh, Elham; Guo, Yue; McGordon, Andrew; Marco, James. 2017. Large format lithium ion pouch cell full thermal characterisation for improved electric vehicle thermal management (2017). Journal of Power Sources. 359.

[3] Erriquez, Mauro; Morel, Thomas; Schäfer, Philip; Moulière, Pierre-Yves. October 2017. Trends in electric-vehicle design. McKinsey & Company, Automotive & Assembly (October 2017). https://www.mckinsey.com/industries/automotive-and-assembly/our-insights/trends-in-electric-vehicle-design.

[4] Alarco, Jose; Talbot, Peter. 2015. The history and development of batteries (2015). https://phys.org/news/2015-04-history-batteries.html#jCp.

[5] Blomgren, George E. 2016. The Development and Future of Lithium Ion Batteries (2016). Journal of The Electrochemical Society. 164.

[6] Nitta, Naoki; Wu, Feixiang; Lee, Jung Tae; Yushin, Gleb. 2015. Li-ion battery materials (2015). Materials Today. 18.

[7] Saha, Bhaskar; Goebel, Kai (2009). Modeling Li-ion battery capacity depletion in a particle filtering framework. https://pdfs.semanticscholar.org/6da6/f559425e9b9f719be1089b3cf254dcc1f8d0.pdf.

[8] Galushkin, N. E.; Yazvinskaya, N. N.; Galushkin, D. N. 2018. Mechanism of Thermal Runaway in Lithium-Ion Cells (2018). Journal of The Electrochemical Society. 165.

[9] Soylu, Seref. 2011. Electric Vehicles â€“ The Benefits and Barriers. 978-953-307-287-6.

[10] Buchmann, Isidor. 2018. BU-205: Types of Lithium-ion. Battery University, Cadex Electronics Inc (2018). http://batteryuniversity.com/learn/article/types_of_lithium_ion.

[11] Padhi, A. K. 1997. Phospho-olivines as Positive-Electrode Materials for Rechargeable Lithium Batteries (1997). Journal of The Electrochemical Society. 144.

[12] Eftekhari, Ali. 2017. LiFePO 4 /C nanocomposites for lithium-ion batteries (2017). Journal of Power Sources. 343.

[13] Athena Combs-Hurtado; Marc Hensel. Memorandum: Using Lithium Iron Phosphate Batteries for Utility Scale Storage Applications. Arizona State University (21 October 2017). http://roedel.faculty.asu.edu/sec598s18/projects/p01_SM.pdf.

[14] Zhang, Xiangwu; Ji, Liwen; Toprakci, Ozan; Liang, Yinzheng; Alcoutlabi, Mataz. 2011. Electrospun Nanofiber-Based Anodes, Cathodes, and Separators for Advanced Lithium-Ion Batteries (2011). Polymer Reviews. 51.

[15] Buchmann, Isidor. 2018. BU-301a: Types of Battery Cells. Battery University, Cadex Electronics Inc (2018). http://batteryuniversity.com/learn/article/types_of_battery_cells.

[16] Schröder, Robert; Aydemir, Muhammed; Seliger, Günther. 2017. Comparatively Assessing different Shapes of Lithium-ion Battery Cells (2017). Procedia Manufacturing. 8.

[17] Jessica Shankleman; Tom Biesheuvel; Joe Ryan; Dave Merrill. 2017. We’re Going to Need More Lithium. Bloomberg LP (2017). https://www.bloomberg.com/graphics/2017-lithium-battery-future/.

[18] AUDI Digital Illustrated. 2016. AUDI future performance 2015 illustrated. AUDI Illustrated (2016). https://www.audi-illustrated.com/en/future-performance-2015/Batterietechnologie.

[19] Jaggi, Anmol. Jan 26, 2017. Comparison of different Li-ion cell types. Gensol Engineering Pvt. Ltd. (Jan 26, 2017). https://www.slideshare.net/AnmolJaggi/comparison-between-different-li-ion-cells-type.

[20] Ahn, Soonho; Lee, Hyang-Mok; Lee, Seung-Jin; Youngsun, Park; Ku, Cha-Hun; Kim, Je Young; Lee, Jae-Hyun; Kim, Seok Koo; Cho, Jin Yeon. The Impact of Cell Geometries and Battery Designs on Safety and Performance of Lithium Ion Polymer Batteries. Batteries R&D, LG Chemical Ltd./ Research Park. https://www.electrochem.org/dl/ma/203/pdfs/0106.pdf.

[21] Maiser, Eric (2014). Battery packaging - Technology review.

[22] Mulder, Grietus; Omar, Noshin; Pauwels, Stijn; Meeus, Marcel; Leemans, Filip; Verbrugge, Bavo; Nijs, Wouter de; van den Bossche, Peter; Six, Daan; van Mierlo, Joeri. 2013. Comparison of commercial battery cells in relation to material properties (2013). Electrochimica Acta. 87.

[23] Zhao, Jingyuan. 2018. Cycle life testing of lithium batteries (2018). International Journal of Electrochemical Science.

[24] Anseán González, David. 2015. High power li-Ion battery performance: a mechanistic analysis of aging (2015).

[25] Barré, Anthony; Deguilhem, Benjamin; Grolleau, Sébastien; Gérard, Mathias; Suard, Frédéric; Riu, Delphine. 2013. A review on lithium-ion battery ageing mechanisms and estimations for automotive applications (2013). Journal of Power Sources. 241.

[26] Sarasketa-Zabala, E.; Gandiaga, I.; Martinez-Laserna, E.; Rodriguez-Martinez, L. M.; Villarreal, I. 2015. Cycle ageing analysis of a LiFePO 4 /graphite cell with dynamic model validations (2015). Journal of Power Sources. 275.

[27] Pinson, M. B.; Bazant, M. Z. 2012. Theory of SEI Formation in Rechargeable Batteries (2012). Journal of the Electrochemical Society. 160. https://arxiv.org/ftp/arxiv/papers/1210/1210.3672.pdf.

[28] Sikha, G.; Ramadass, P.; Haran, B. S.; White, R. E.; Popov, Branko N. 2003. Comparison of the capacity fade of Sony US 18650 cells charged with different protocols (2003). Journal of Power Sources. 122.

[29] Han, Xuebing; Ouyang, Minggao; Lu, Languang; Li, Jianqiu; Zheng, Yuejiu; Li, Zhe. 2014. A comparative study of commercial lithium ion battery cycle life in electrical vehicle (2014). Journal of Power Sources. 251.

[30] Sun, Shun; Guan, Ting; Shen, Bin; Leng, Kunyue; Gao, Yunzhi; Cheng, Xinqun; Yin, Geping. 2017. Changes of Degradation Mechanisms of $LiFePO_4$ /Graphite Batteries Cycled at Different Ambient Temperatures (2017). Electrochimica Acta. 237.

[31] Lewerenz, Meinert; Marongiu, Andrea; Warnecke, Alexander; Sauer, Dirk Uwe. 2017. Differential voltage analysis as a tool for analyzing inhomogeneous aging (2017). Journal of Power Sources. 368.

[32] Uddin, Kotub; Perera, Surak; Widanage, W.; Somerville, Limhi; Marco, James. 2016. Characterising Lithium-Ion Battery Degradation through the Identification and Tracking of Electrochemical Battery Model Parameters (2016). Batteries. 2.

[33] Frank Kindermann. 2012. The Solid-Electrolyte Interface.

[34] Xu, Kang. 2004. Nonaqueous Liquid Electrolytes for Lithium-Based Rechargeable Batteries (2004). Chemical Reviews. 104.

[35] DuBeshter, Tyler; Jorne, Jacob. 2017. Pulse Polarization for Li-Ion Battery under Constant State of Charge (2017). Journal of The Electrochemical Society. 164.

[36] Liu, Chaofeng; Neale, Zachary G.; Cao, Guozhong. 2016. Understanding electrochemical potentials of cathode materials in rechargeable batteries (2016). Materials Today. 19. https://www.sciencedirect.com/science/article/pii/S1369702115003181.

[37] Park, Myounggu; Zhang, Xiangchun; Chung, Myoungdo; Less, Gregory B.; Sastry, Ann Marie. 2010. A review of conduction phenomena in Li-ion batteries (2010). Journal of Power Sources. 195.

[38] Zhou, Daming; Zhang, Ke; Ravey, Alexandre; Gao, Fei; Miraoui, Abdellatif. 2016. Parameter Sensitivity Analysis for Fractional-Order Modeling of Lithium-Ion Batteries (2016). Energies. 9.

[39] Barai, Anup; Uddin, Kotub; Widanage, W. D.; McGordon, Andrew; Jennings, Paul. 2018. A study of the influence of measurement timescale on internal resistance characterisation methodologies for lithium-ion cells (2018). Scientific reports. 8.

[40] Jow, T. Richard; Delp, Samuel A.; Allen, Jan L.; Jones, John-Paul; Smart, Marshall C. 2018. Factors Limiting Li + Charge Transfer Kinetics in Li-Ion Batteries (2018). Journal of The Electrochemical Society. 165.

[41] Jow, T. R.; Allen, Jan L.; Deveney, Bridget; Nechev, Kamen (October 12 - October 17, 2008). Charge Transfer and Charge-Discharge Kinetics in Lithium-ion Batteries.

[42] Valøen, Lars Ole; Reimers, Jan N. 2005. Transport Properties of LiPF[sub 6]-Based Li-Ion Battery Electrolytes (2005). Journal of The Electrochemical Society. 152.

[43] Lundgren, Henrik. 2015. Thermal aspects and electrolyte mass transport in lithium-ion batteries. TRITA-CHE-Report. 2015:22. 978-91-7595-584-1.

[44] Gao, Jian; Shi, Si-Qi; Li, Hong. 2015. Brief overview of electrochemical potential in lithium ion batteries (2015). Chinese Physics B. 25.

[45] Palcoux, G.; Schmalz, J.; Richter, L.; Porcher, W. SPICY Deliverable D5.6. CEA, TUM-PROLLION.

[46] Yaakov, David; Gofer, Yossi; Aurbach, Doron; Halalay, Ion C. 2010. On the Study of Electrolyte Solutions for Li-Ion Batteries That Can Work Over a Wide Temperature Range (2010). Journal of The Electrochemical Society. 157.

[47] Trad, Khiem; Mulder, Grietus; Gutiérrez, César; Meatza, Iratxe de; Delaille, Arnaud; Porcher, Willy. SPICY Deliverable D6.1. CIDETEC, CEA, TUM, PROLLION.

[48] M. Nisvo Ramadan; Bhisma A. Pramana; Adha Cahyadi; Oyas Wahyunggoro. 2016. State of health estimation in lithium polymer battery.

[49] Li, Lian-xing; Tang, Xin-cun; Qu, Yi; Liu, Hong-tao. 2011. CC-CV charge protocol based on spherical diffusion model (2011). Journal of Central South University of Technology. 18.

[50] Svens, Pontus; Behm, Mårten; Lindbergh, Göran. 2015. Lithium-Ion Battery Cell Cycling and Usage Analysis in a Heavy-Duty Truck Field Study (2015). Energies. 8.

[51] Liu, Guang; Guo, Liang; Liu, Chunlong; Wu, Qingwen. 2018. Evaluation of different calibration equations for NTC thermistor applied to high-precision temperature measurement (2018). Measurement. 120.

[52] Chang, Wen-Yeau. 2013. The State of Charge Estimating Methods for Battery (2013). ISRN Applied Mathematics. 2013.

[53] Zhao, Rui; Zhang, Sijie; Gu, Junjie; Liu, Jie. 2016. 2016 IEEE Electrical Power and Energy Conference (EPEC). IEEE Electrical Power and Energy Conference; Annual IEEE Electrical Power and Energy Conference; Conférence sur l'énergie électrique de l'IEEE; EPEC. 978-1-5090-1919-9.

[54] Novais, Susana; Nascimento, Micael; Grande, Lorenzo; Domingues, Maria Fátima; Antunes, Paulo; Alberto, Nélia; Leitão, Cátia; Oliveira, Ricardo; Koch, Stephan; Kim, Guk Tae; Passerini, Stefano; Pinto, João. 2016. Internal and External Temperature Monitoring of a Li-Ion Battery with Fiber Bragg Grating Sensors (2016). Sensors (Basel, Switzerland). 16.

[55] An, Seong Jin; Li, Jianlin; Daniel, Claus; Mohanty, Debasish; Nagpure, Shrikant; Wood, David L. 2016. The state of understanding of the lithium-ion-battery graphite solid electrolyte interphase (SEI) and its relationship to formation cycling (2016). Carbon. 105.

[56] Wu, Yao; Keil, Peter; Schuster, Simon F.; Jossen, Andreas. 2017. Impact of Temperature and Discharge Rate on the Aging of a LiCoO 2 /LiNi 0.8 Co 0.15 Al 0.05 O 2 Lithium-Ion Pouch Cell (2017). Journal of The Electrochemical Society. 164.

[57] Lewerenz, Meinert; Münnix, Jens; Schmalstieg, Johannes; Käbitz, Stefan; Knips, Marcus; Sauer, Dirk Uwe. 2017. Systematic aging of commercial LiFePO 4

|Graphite cylindrical cells including a theory explaining rise of capacity during aging (2017). Journal of Power Sources. 345.

[58] Friesen, Alex; Mönnighoff, Xaver; Börner, Markus; Haetge, Jan; Schappacher, Falko M.; Winter, Martin. 2017. Influence of temperature on the aging behavior of 18650-type lithium ion cells (2017). Journal of Power Sources. 342.

List of Figures

List of Tables